Structural Consequences of the Range of the Interatomic Potential: a Menagerie of Clusters

Jonathan P. K. Doye* and David J. Wales
University Chemical Laboratory, Lensfield Road, Cambridge CB2 1EW, UK
(September 19, 1997)

We have attempted to find the global minima of clusters containing between 20 and 80 atoms bound by the Morse potential as a function of the range of the interatomic force. The effect of decreasing the range is to destabilize strained structures, and hence the global minimum changes from icosahedral to decahedral to face-centred-cubic as the range is decreased. For $N > 45$ the global minima associated with a long-ranged potential have polytetrahedral structures involving defects called disclination lines. For the larger clusters the network of disclination lines is disordered and the global minimum has an amorphous structure resembling a liquid. The size evolution of polytetrahedral packings enables us to study the development of bulk liquid structure in finite systems. As many experiments on the structure of clusters only provide indirect structural information, these results will be very useful in aiding the interpretation of experiment. They also provide candidate structures for theoretical studies using more specific and computationally expensive descriptions of the interatomic interactions. Furthermore, Morse clusters provide a rigorous testing ground for global optimization methods.

I. INTRODUCTION

Structural information is of fundamental importance in addressing the chemical and physical properties of any system. Unfortunately, there is no direct experimental method for determining the structure of free clusters in molecular beams. Instead, one measures properties which depend on structure and employs models of the predicted favoured geometries. This approach has been combined with techniques such as electron diffraction,[1] mass spectral abundances,[2] chemical reactivity,[3] magnetism[4] and x-ray spectroscopy.[5] The inversion of the experimental data to obtain structural information, though, can be problematic, and always relies on comparisons with the predictions of structural models.

Sizes exhibiting special stability are known for certain morphologies and classes of interatomic potential.[6,7] The size-dependence of properties sometimes reveals these magic numbers, and thus enables a confident structural assignment to be made. However, often rather little is known about the structure between these magic numbers. One of the most powerful experimental techniques that addresses this deficiency is the flow-reactor approach which probes the chemical reactivity of size-selected clusters. For example, this method has been applied to nickel clusters to give detailed information for all sizes up to N=71.[8–11] The results show that around N=13 and N=55 the clusters are icosahedral, in agreement with the observed magic numbers in other experiments.[4,12,13] However, in the size range $29 < N < 48$ only one structural assignment has so far been made because of the large number of possible geometries to be considered and the presence of multiple isomers.[11]

The theoretician can aid in the task of structural assignment by providing realistic candidate structures. Indeed, many studies have modelling specific clusters, but *ab initio* calculations are only feasible for small sizes, especially for transition metals, and so empirical potentials are often used. However, as is clear from the diversity of theoretical results obtained for nickel clusters,[14–20] consensus between methods is lacking and it is hard to know which (if any) of the results should be believed. Even with the simplified description of the interatomic interactions provided by an empirical potential, it can be an extremely difficult task to search the potential energy surface (PES) extensively enough to be confident that the global minimum has been found. Also, many empirical potentials are too complicated to provide an understanding of the relationship between the potential and the observed structure and so little physical insight is gained.

Therefore, to understand cluster structure there is a need for a hierarchy of theoretical models from the general to the specific. In the present study we use a simple model to understand the structural effects of the range of the potential, and so provide one part of the framework for understanding the physical basis of cluster structure. We are confident that we have found most of the global minima giving the most comprehensive model of cluster structure in the small size regime.

*Present Address: FOM Institute for Atomic and Molecular Physics, Kruislaan 407, 1098 SJ Amsterdam, The Netherlands

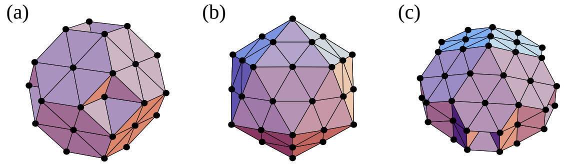

FIG. 1. (a) 38-atom truncated octahedron, (b) 55-atom Mackay icosahedron, and (c) 75-atom Marks decahedron. These clusters have optimal shapes for the three main types of ordered packing seen in clusters: face-centred cubic (fcc), icosahedral and decahedral, respectively. The latter two morphologies cannot be extended to the bulk because of the five-fold axes of symmetry.

One of the most interesting aspects of cluster structure is the manifestation of non-crystallographic symmetries which arise from the absence of translational periodicity. In particular, many clusters are found to have fivefold axes of symmetry, including two of the three main types of ordered structure adopted by simple atomic clusters. Decahedra have a single fivefold axis of symmetry and are based on pentagonal bipyramids, while icosahedra have six fivefold axes of symmetry. The third morphology consists of close-packed clusters. Particularly stable examples of each type are illustrated in Fig. 1.

All the above morpholgies have been observed experimentally. Many gas phase clusters have been shown to be icosahedral through the presence of the magic numbers associated with the Mackay icosahedra[21] in mass spectra: rare gases[22–24], metals,[13,25–27] and molecular clusters.[28,29] Icosahedral and decahedral structures are also commonly reported for metal clusters supported on surfaces,[30] and more recently fcc and decahedral clusters have been observed for gold clusters passivated by alkylthiolates.[31–35]

All three structural types are also exhibited by Lennard-Jones (LJ) clusters. For $N < 1600$ icosahedra are most stable; from this size up to $N \approx 10^5$ decahedra are most stable and above this fcc clusters.[36] However, these changes do not occur abruptly. The global minimum of LJ_{38} is the fcc truncated octahedron[37,38] (Fig. 1(a)) and for at least six sizes with $N < 110$ the global minimum is based upon a Marks decahedron[7,38] (Fig. 1(c)). In this paper we consider a potential with variable range to provide a model system which exhibits a much greater diversity of structural behaviour than LJ clusters in the small size regime. Consequently, the results are relevant to a much wider range of systems.

There have been a number of previous studies on the effect of the range of the potential on the structure and phase behaviour of small clusters.[38–45] These have shown that the number of minima and saddle points on the PES increases as the range decreases—the PES becomes more rugged[39,42,46,47]—and strained structures are destabilized. The latter effect results in range-induced transitions between the ordered morphologies,[38] and the destabilization and disappearance of the liquid phase as the range is decreased.[41,42,48] In a previous paper we examined Morse clusters containing up to 25 atoms and a selection of larger sizes.[38] Here we consider Morse clusters in the size range $20 < N \leq 80$ atoms. Some of the lowest energy structures given here supersede the results of the previous paper.

II. METHODS

A. The potential

The Morse potential[49] may be written as

$$V_M = \epsilon \sum_{i<j} e^{\rho_0(1-r_{ij}/r_0)}(e^{\rho_0(1-r_{ij}/r_0)} - 2), \qquad (1)$$

where ϵ is the pair well depth and r_0 the equilibrium pair separation. We denote an N-atom cluster bound by the Morse potential as M_N. In reduced units ($\epsilon = 1$ and $r_0 = 1$) there is a single adjustable parameter, ρ_0, which determines the range of the interparticle forces. Fig. 2 shows that decreasing ρ_0 increases the range of the attractive part of the potential and softens the repulsive wall, thus widening the potential well. Values of ρ_0 appropriate to a range of materials have been catalogued elsewhere.[50] The LJ potential has the same curvature at the bottom of the well as the Morse potential when $\rho_0 = 6$. Girifalco has obtained an intermolecular potential for C_{60} molecules[51] which is isotropic and short-ranged relative to the equilibrium pair separation, with an effective value of $\rho_0 = 13.62$.[52] The alkali metals have longer-ranged interactions, for example ρ_0=3.15 has been suggested for sodium.[53] Fitting to bulk data gives a value of ρ_0=3.96 for nickel.[14]

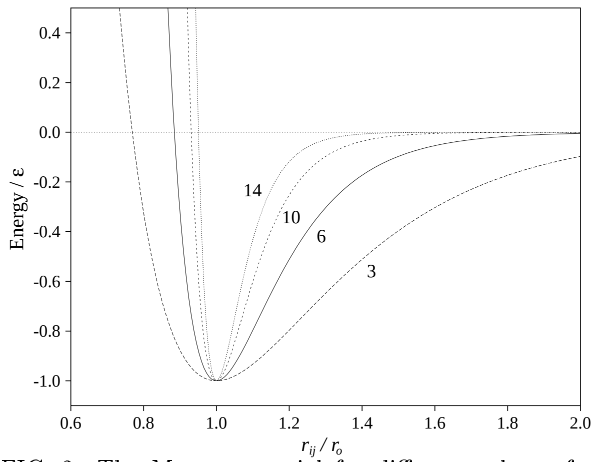

FIG. 2. The Morse potential for different values of the range parameter ρ_0 as indicated.

At absolute zero the structure with the lowest free energy is simply the global potential energy minimum of the PES. At higher temperatures, entropic factors must also be considered. Although we only perform a comprehensive survey of the zero Kelvin geometries, the structural effects of temperature are considered in the subsequent discussion.

To understand the structural effects of the range parameter, ρ_0, it is instructive to look more closely at the form of the potential. The energy can be partitioned into three contributions:

$$V_M = -n_{nn}\epsilon + E_{\rm strain} + E_{nnn}. \tag{2}$$

The number of nearest-neighbour contacts, n_{nn}, the strain energy, $E_{\rm strain}$, and the contribution to the energy from non-nearest neighbours, E_{nnn}, are given by

$$\begin{aligned} n_{nn} &= \sum_{i<j, x_{ij}<x_0} 1, \\ E_{\rm strain} &= \epsilon \sum_{i<j, x_{ij}<x_0} (e^{-\rho_0 x_{ij}} - 1)^2, \\ E_{nnn} &= \epsilon \sum_{i<j, x_{ij}>x_0} e^{-\rho_0 x_{ij}}(e^{-\rho_0 x_{ij}} - 2), \end{aligned} \tag{3}$$

where $x_{ij} = r_{ij}/r_0 - 1$, and x_0 is a nearest-neighbour criterion. x_{ij} is the strain in the contact between atoms i and j.

The dominant term in the energy comes from n_{nn}. E_{nnn} is a smaller term and its value varies in a similar manner to n_{nn}. It is only likely to be important in determining the lowest energy structures when other factors are equal. For example, bulk fcc and hexagonal close-packed (hcp) lattices both have twelve nearest neighbours per atom. Next-nearest neighbour interactions are the cause of the lower energy of the hcp crystal when a pair potential such as the LJ form is used.[54,55]

$E_{\rm strain}$, which measures the energetic penalty for the deviation of a nearest-neighbour distance from the equilibrium pair distance, is a key quantity in our analysis. It must not be confused with strain due to an applied external force. For a given geometry, $E_{\rm strain}$ grows rapidly with increasing ρ_0 because the potential well narrows. To a first approximation the strain energy grows quadratically with ρ_0.[38] Hence, decreasing the range destabilizes strained structures.

From the above analysis we can see that minimization of the potential energy involves a balance between maximizing n_{nn} and minimizing $E_{\rm strain}$. The interior atoms of the three morphologies (Fig. 1) all have twelve nearest neighbours, and so differences in n_{nn} arise from surface effects. The optimal shape for each morphology results from the balance between maximizing the proportion of {111} faces (an atom in a {111} face is 9-coordinate, but in a {100} face only 8-coordinate) and minimizing the fraction of atoms in the surface layer. As Mackay icosahedra (Fig. 1(b)) have only {111} faces and are approximately spherical, the icosahedra have the largest n_{nn}. Complete Mackay icosahedra occur at $N = 13, 55, 147, \ldots$ A pentagonal bipyramid has only {111} faces, but because it is not very spherical more stable decahedral forms are obtained by truncating the structure parallel to the five-fold axis to reveal five {100} faces and then introducing re-entrant {111} faces between adjacent {100} faces. The resulting structure is called a Marks decahedron (Fig. 1(c)) and was first predicted by the use of a modified Wulff construction.[56] Decahedra generally have lower values of n_{nn} than icosahedra because of the {100} faces. The tetrahedron and octahedron are fcc structures that have only {111} faces, but they are not very spherical. The optimal fcc structure is the truncated octahedron with regular hexagonal faces (Fig. 1(a)). At larger sizes than those considered in this study, the optimal structure involves further facetting, so that it more closely approximates the Wulff polyhedron.[57] Of the three morphologies fcc structures have the smallest values of n_{nn}.

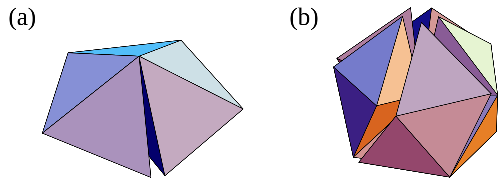

FIG. 3. Examples of the strain involved in packing tetrahedra. (a) Five regular tetrahedra around a common edge produce a gap of 7.36°. (b) Twenty regular tetrahedra about a common vertex produce gaps equivalent to 1.54 steradians.

A Mackay icosahedron can be decomposed into twenty fcc tetrahedra, but as we see from Fig. 3(b), when twenty regular tetrahedra are packed around a common vertex large gaps remain. To bridge these gaps the tetrahedra have to be distorted, thus introducing strain. The distance between adjacent vertices of the icosahedron is 5% larger than the distance between a vertex and the centre. Similarly, a pentagonal bipyramid can be decomposed into five fcc tetrahedra sharing a common edge. Again, a gap remains if regular tetrahedra are used (Fig. 3(a)) and consequently decahedral structures are strained, although not as much as icosahedra. In contrast, close-packed structures can be unstrained.

Having deduced the relative values of n_{nn} and $E_{\rm strain}$ for icosahedral, decahedral and fcc structures, we can predict the effect of the range on the competition between them. For a moderately long-ranged potential, the strain associated with the icosahedron can be accommodated without too large an energetic penalty and so such structures are the most stable. As the range of the potential is decreased, the strain energy associated with icosahedra increases rapidly, and there comes a point where decahedra become more stable. Similarly, for a sufficiently short-ranged potential fcc structures become more stable than decahedral structures.

The above decomposition of the potential energy also helps us to understand the effect of size on the energetic competition between the three morphologies. The differences in n_{nn}, which arise from the different surface structures, are approximately proportional to the surface area ($\propto N^{2/3}$). The strain energies, however, are proportional to the volume ($\propto N$). Therefore, the differences in $E_{\rm strain}$ increase more rapidly with size than the differences in n_{nn}, thus explaining the change in the most stable morphology from icosahedral to decahedral to fcc with increasing size. The effect of increasing the size is similar to the effect of decreasing the range of the potential: both destabilize strained structures.

B. Searching the potential energy surface

The principal method that we have used to generate candidate structures for the global minima makes use of the physical insight gained from the last section. We have simply attempted to construct geometries that maximize n_{nn} for the three ordered morphologies.[7] The resulting structures were then optimized by either conjugate gradient[58] or eigenvector-following[59] methods. A similar approach was successfully used by Northby to generate low energy icosahedra for LJ clusters.[6] The effectiveness of this method is demonstrated by how few of Northby's lowest energy structures have been superseded and by the length of time that it has taken to find these exceptions.[7,37,38,60–63] Our approach, however, depends on the imagination of the practitioner to conceive of all the possible ways that a structure with a large value of n_{nn} could be obtained. Furthermore, this method will always fail to find the global minimum if the latter is not based on one of the ordered structures, as is the case for the larger clusters we have considered at low values of ρ_0.

To complement the above approach two global optimization techniques were used to try to find structures that might have been missed. Firstly, we used a method in which eigenvector-following is employed to take steps directly between minima on the PES.[64,65] If low temperature Metropolis Monte Carlo is used in this space of minima, the system will walk down to the bottom of a basin containing many minima. This technique avoids the difficulties associated with trapping in local minima that can occur for methods which take steps directly in configuration space. Secondly, we used a 'basin hopping' approach, which has proved to be effective for LJ clusters;[63,66] it is the only unbiased global optimization method to have found the global minima that are Marks decahedra. For Morse clusters it was able to find all the lowest energy minima at ρ_0=3, 6, 10 and all but twelve at ρ_0=14; this included some structures that were lower than any of those we had constructed. The fact that we found most of the minima both by unbiased global optimization and by construction makes us confident that our lowest energy structures are truly global minima.

The results for the basin-hopping algorithm are impressive because the global optimization task for Morse clusters is a difficult one. The size of the configuration space for the larger clusters is compounded for short-ranged potentials by the nature of the PES. Firstly, the PES becomes more rugged as the range is decreased.[42] The physical reason for the larger number of minima at short range is the loss of accessible configuration space as the potential wells become narrower, producing barriers where there are none at long range. Stillinger and Stillinger[67] and Bytheway and Kepert[40] both found that minimizations performed from random starting configurations are much less likely to find the global minimum for a short-ranged potential.

Similarly, barrier heights are also likely to become higher and rearrangements more localized for a shorter-ranged potential. These trends have been observed in comparisons of the rearrangements of 55-particle C_{60} and LJ clusters.[68] Hence the range of the potential is likely to have a significant impact on the dynamics, making escape from local minima much more difficult. This effect has been observed by Rose and Berry who have shown that the rate at which the ground state structure of a potassium chloride cluster is found upon cooling can be significantly decreased by using a shielded Coulomb potential to reduce the range of the interactions.[69]

Furthermore, as a result of the competition between the decahedral and the various types of close-packed structures for short-ranged potentials, it is more likely that there are a number of low energy minima which are very close in energy but are structurally dissimilar. Each of these minima lie at the bottom of their own funnel on the PES. This multiple funnel topography can lead to cases where optimization is extremely difficult because the free energy barriers for transitions between the funnels can be large, thus leading to trapping. The worst cases are when relaxation down the PES preferentially takes the system into a funnel which does not end at the global minimum,[70] and when the global minimum only becomes the state with the lowest free energy at low temperatures.[66]

Finally, fcc and decahedral minima are more structurally dissimilar from minima typical of the liquid-like state than the icosahedral structures. Therefore, the paths from the liquid to these structures are likely to be fewer and longer than those leading to the icosahedral structures,[64] and so relaxation down the PES from the liquid-like state to fcc and decahedral global minima is harder.

For a number of reasons Morse clusters are an ideal system with which to test global optimization methods designed for configurational problems. Firstly, in this paper we provide very good estimates for the energies of the global minima. Secondly, this system represents a much more general—the global minima have a variety of structural types—and tougher examination than is provided by LJ clusters, a much-used test system for global optimization algorithms.[63] And finally, the results for our basin-hopping algorithm provide a benchmark that any would-be global optimization method should try to beat.

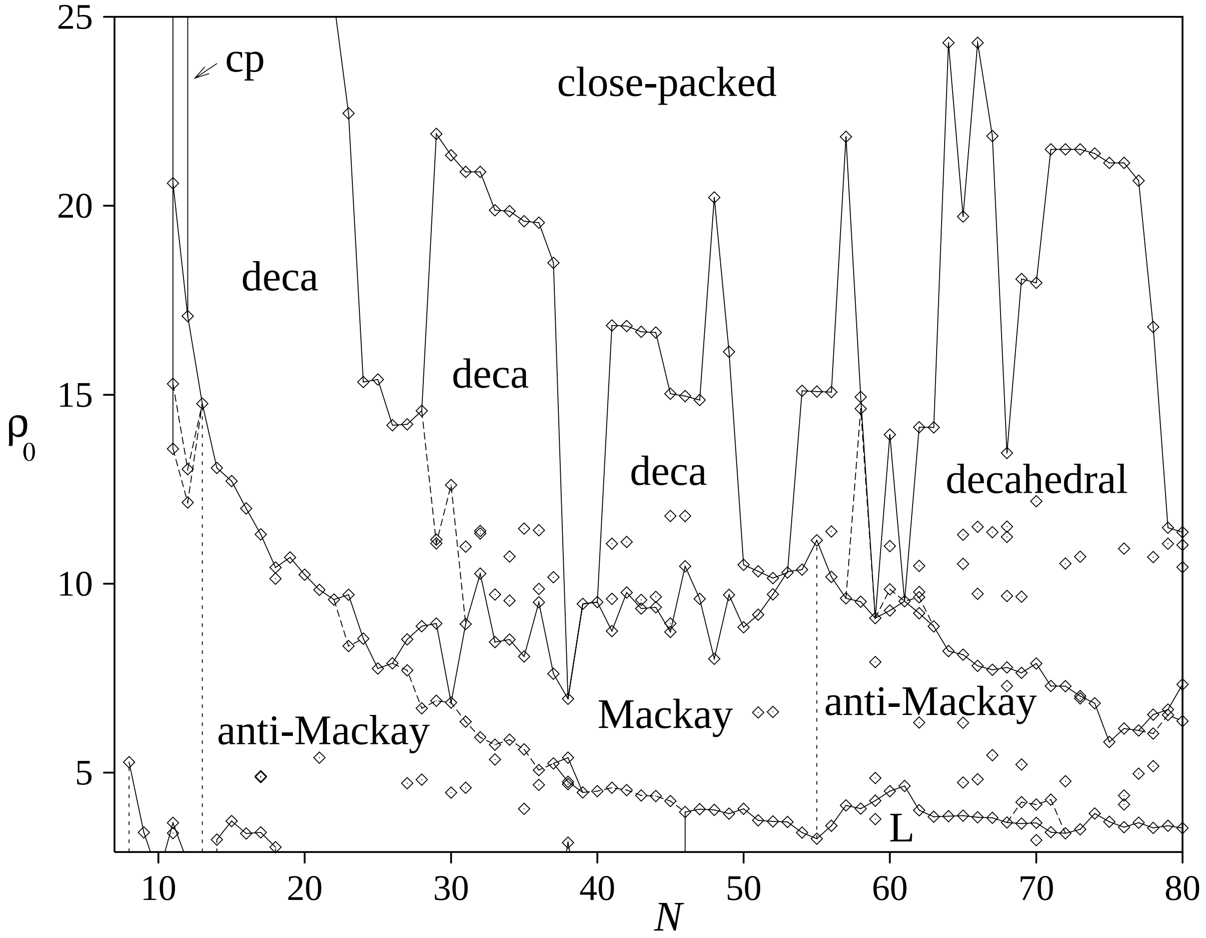

FIG. 4. Zero temperature 'phase diagram' showing the variation of the lowest energy structure with N and ρ_0. The data points are the values of ρ_0 at which the global minimum changes. The lines joining the data points divide the phase diagram into regions where the global minima have similar structures. The solid lines denote the boundaries between the four main structural types—icosahedral, decahedral, close-packed and those associated with low ρ_0 (L)—and the dashed lines are internal boundaries within a structural type, e.g. between icosahedra with Mackay and anti-Mackay overlayers, or between decahedra with different length decahedral axes.

III. RESULTS

All the global minima that we have found are catalogued in Table 1 along with their energies, point groups, number of nearest neighbours, strain energies and the values of ρ_0 for which they are probably the lowest energy minimum.

The results are summarized in Fig. 4 which provides a zero temperature 'phase diagram', showing how the global minimum depends upon N and ρ_0. The structural behaviour of Morse clusters with fewer than eight atoms is rather uninteresting because the global minimum is independent of ρ_0. For all $N \geq 8$, however, the global minimum changes at least once as a function of ρ_0. For $N \geq 13$, icosahedral, decahedral and fcc structures all exist, and the form of the phase diagram is in good agreement with the predictions we made earlier based upon the decomposition of the potential energy. For most sizes the structure changes from icosahedral to decahedral to close-packed as the range of the potential is decreased. For $N < 23$, however, the transition from decahedral to close-packed occurs at larger values of ρ_0 than we consider in this study. There are also a number of sizes (N=38–40, 52, 53, 59 and 61) for which there is a transition directly from an icosahedral to a close-packed structure; this occurs when n_{nn} for the lowest energy close-packed structure is greater than or equal to that for the lowest energy decahedron.

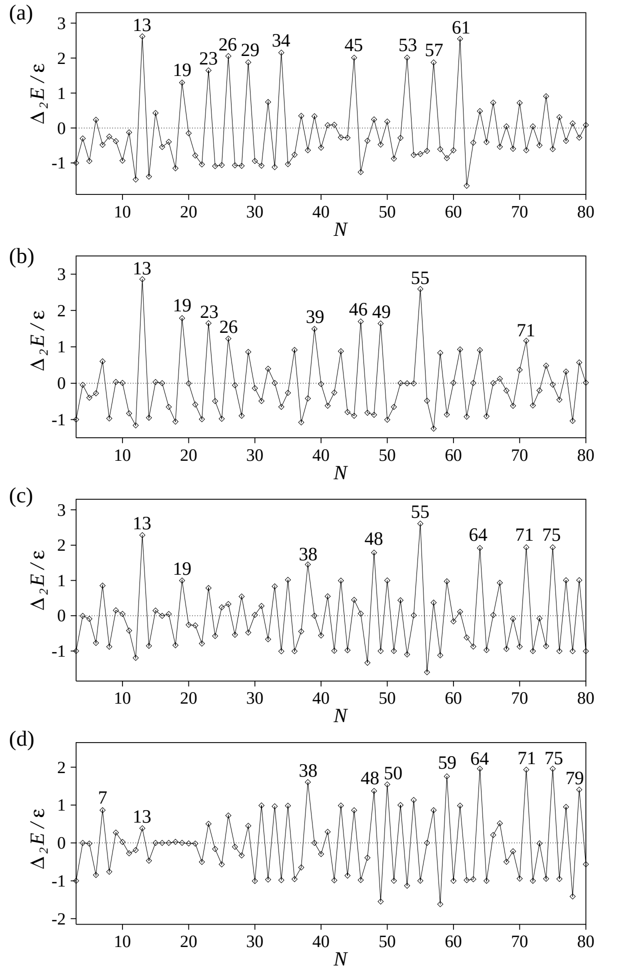

FIG. 5. Plots of $\Delta_2 E$ as a function of N for (a) ρ_0=3, (b) ρ_0=6, (c) ρ_0=10 and (d) ρ_0=14.

The boundaries between the different morphologies are sensitive functions of N. Such size dependence is observed for many properties of clusters, and gradually lessens as N increases (because the addition of a single atom becomes a smaller perturbation) until the bulk limit is reached. The decahedral to close-packed boundary is particularly sensitive, because the range of ρ_0 for which the decahedron is most stable changes dramatically even when the difference in n_{nn} between the decahedral and close-packed structures changes by one.

Sizes for which a morphology is the lowest in energy for a particularly large range of ρ_0 indicate that the structure is especially stable. The optimal geometries shown in Fig. 1 are good examples. Another indicator of special stability is provided by $\Delta_2 E(N) = E(N+1) + E(N-1) - 2E(N)$. Peaks in $\Delta_2 E$ have been found to correlate well with the magic numbers (sizes at which clusters are particularly abundant) observed in mass spectra.[71] Plots of $\Delta_2 E$ are shown in Fig. 5 for a number of values of ρ_0. Unsurprisingly, the plot for ρ_0=6 is very similar to that for LJ clusters with peaks due to especially stable icosahedral clusters. At higher values of ρ_0 peaks corresponding to close-packed and decahedral clusters begin to occur. The plot at ρ_0=14 is very similar to that recently obtained for C_{60} clusters using the Girifalco intermolecular potential.[72] If the energy is 'normalized' by subtracting a suitable function of N, particularly stable sizes again stand out (Fig. 6).

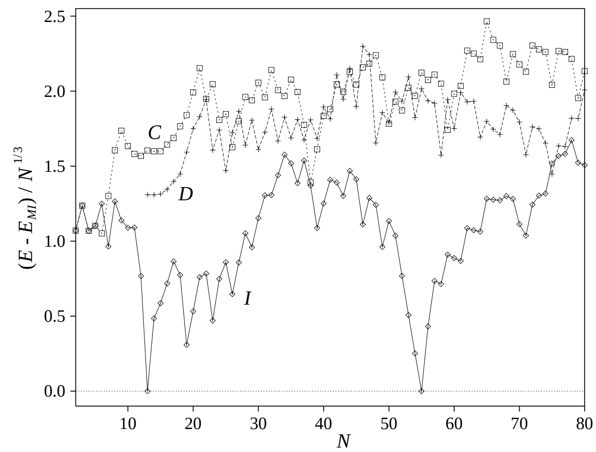

FIG. 6. Comparison of the energies of icosahedral (solid line with diamonds), decahedral (dashed line with crosses) and close-packed (dotted line with squares) M_N clusters at ρ_0=6. The energy zero is E_{MI}, the interpolated energy of Mackay icosahedra. $E_{MI} = -3.0354 + 0.2624N^{1/3} + 8.8400N^{2/3} - 6.8381N$ and was obtained by fitting to the first four Mackay icosahedra (N=13, 55, 147 and 309).

In the following subsections we will look at the growth sequences for each morphology in more detail. We also examine the unusual structures that occur for the larger clusters at low ρ_0, which, as we will see, involve a mixture of order and disorder.

A. Icosahedral clusters

Many small clusters are polytetrahedral in the sense that the whole of the cluster can be divided into tetrahedra. This category includes the 13-atom icosahedron, which can be decomposed into twenty tetrahedra sharing a common vertex. Addition of atoms to the icosahedron can occur in two ways and the two types of overlayer that result are illustrated in Fig. 7. One growth mode (fcc-like) continues the fcc packing of the twenty strained tetrahedra making up the icosahedron, and leads to the 55-atom Mackay icosahedron (Fig. 1(b)). This scheme introduces octahedral interstices, and so the resulting structures are no longer polytetrahedral. The other 'anti-Mackay' (hcp-like) growth mode involves sites which are hcp with respect to the tetrahedra. For growth on the 13-atom icosahedron, this overlayer preserves polytetrahedral character. Each of the vertices of the original icosahedron becomes icosahedrally coordinated, and the structure that results from the completion of this overlayer, 45A, is a rhombic tricontahedron; it is an icosahedron of interpenetrating icosahedra. Interestingly, the rhombic tricontahedron is the face-dual of the truncated icosahedron made famous by C_{60}; indeed, it is even a particularly stable shell for the coverage of a C_{60} molecule by alkaline earth metal atoms.[73] In previous studies, the anti-Mackay overlayer has been referred to as the polyicosahedral[1] or the face-capping overlayer.[6] Such names are reasonable for growth on the 13-atom icosahedron, but are confusing for growth on larger Mackay icosahedra.

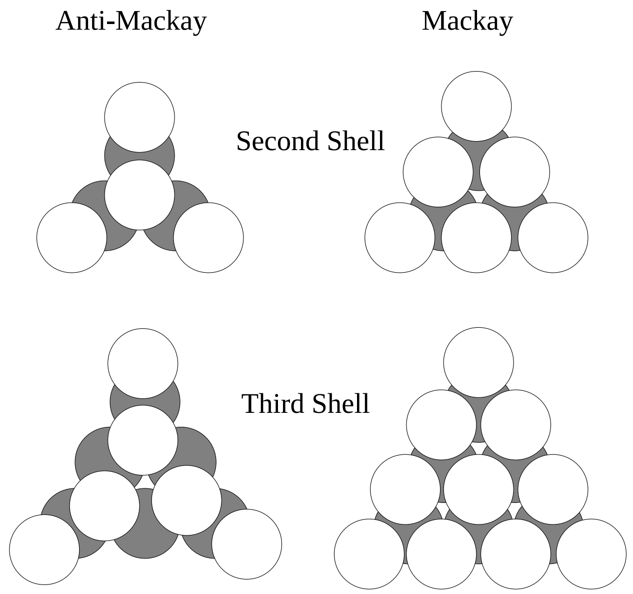

FIG. 7. Atomic positions for the two possible overlayers of the icosahedron, anti-Mackay (left) and Mackay (right). These are shown for a single face of the icosahedron.

The icosahedral structures with an anti-Mackay overlayer are illustrated in Fig. 8 and those with a Mackay overlayer in Fig. 9. Growth from the 13-atom icosahedron begins in the anti-Mackay positions, because these do not include any low-coordinate edge sites, thus giving a larger n_{nn}. However, at some critical size the Mackay overlayer becomes lower in energy because of the larger strain energies associated with the anti-Mackay overlayer. Further growth then leads to the next Mackay icosahedron. The size at which this change occurs depends on the range of the potential; it is given by the dashed line of negative slope that divides the icosahedral region of the phase diagram (Fig. 4). The crossover size increases with the range of the potential.

At $\rho_0 = 6$ the Mackay overlayer is the lowest in energy for $N \geq 32$; the corresponding result for LJ clusters is $N \geq 31$. In *ab initio* molecular dynamics calculations for lithium clusters,[74] the anti-Mackay overlayer is lowest in energy up to $N = 45$. Similarly, polytetrahedral structures were observed in a tight-binding study of sodium clusters up to the largest size considered N=34 (for which 34A was the most stable structure).[75] These effects are nicely explained by the long range of alkali metal potentials.

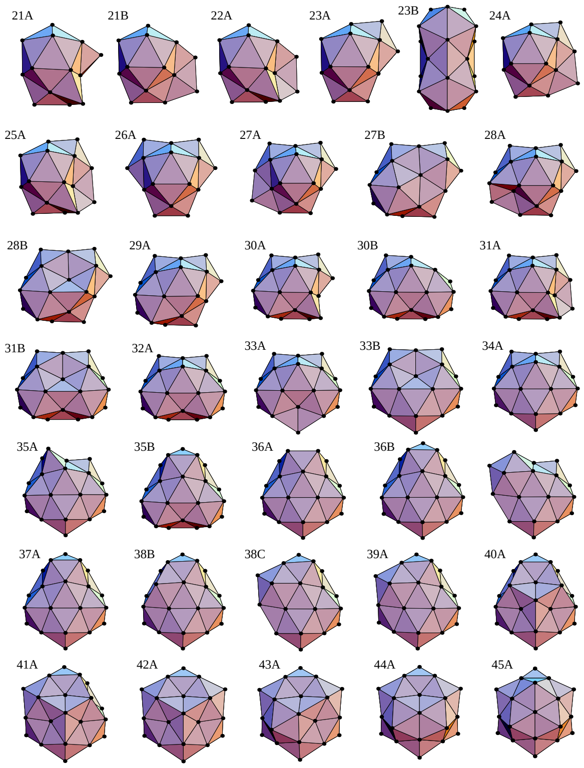

FIG. 8. Icosahedral global minima formed by growth of an anti-Mackay overlayer on the 13-atom icosahedron, except structure 23B which is composed of two face-sharing icosahedra.

Especially stable structures with an anti-Mackay overlayer occur when the icosahedral coordination of a vertex atom is complete. These structures give rise to the peaks in $\Delta_2 E$ at N=19, 23 26, 29, 34 and 45 for ρ_0=3; only the first four of these peaks are seen at ρ_0=6, and only the first at ρ_0=10 (Fig. 5). Some of these magic numbers have been observed in the mass spectra of noble gases[22–24] and even barium.[76] The centres of the icosahedra in these structures form a dimer for 19A, an equilateral triangle for 23A, a tetrahedron for 26A, a trigonal bipyramid for 29A, a pentagonal bipyramid for 34A, and an icosahedron for 45A.

At a number of sizes there is more than one global minimum with an anti-Mackay overlayer for different values of ρ_0. The transitions between these structures are related to small differences in the value of E_{strain}. Also illustrated in Fig. 8 is structure 23B, which is made up of two face-sharing icosahedra. It can be formed from structure 17B by the addition of six atoms to part of the overlayer.

The first global minimum with a Mackay overlayer occurs at N=27. Especially stable structures occur at those sizes for which complete faces of the 55-atom Mackay icosahedra are missing. These structures give rise to the peaks at N=39, 46 and 49 for ρ_0=6 and correspond to 5, 2 and 1 missing faces, respectively. Again, these magic numbers have been seen in the mass spectra of noble gases.[23]

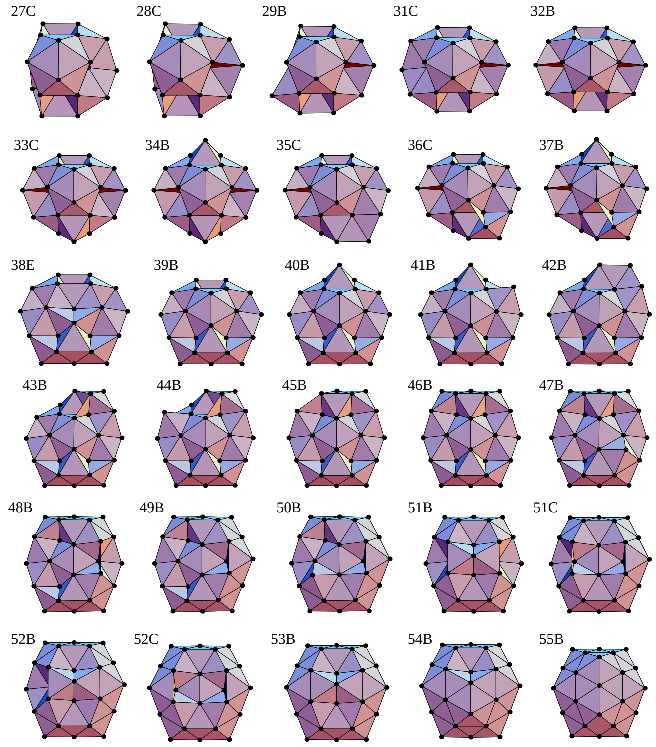

FIG. 9. Icosahedral global minima formed by growth of a Mackay overlayer on the 13-atom icosahedron.

Structure 38E has an atom missing from a vertex of the original 13-atom icosahedron to allow the overlayer to complete a particularly stable form. This structure was not found in Northby's study, but it is the lowest energy LJ icosahedral cluster.[62]

The icosahedral global minima with more than 55 atoms are shown in Fig. 10. As for the 13-atom icosahedron, growth initially occurs at the anti-Mackay sites, because this results in structures with larger n_{nn}. Completion of this overlayer occurs for a cluster with 127 atoms. The vertices of the 55-atom Mackay icosahedron become icosahedrally coordinated, but the edge atoms have a decahedral coordination shell (this is clearly visible for 59D) leading to the half octahedra that are visible in the surface layers of the anti-Mackay clusters. The most prominent peak in $\Delta_2 E$ due to an anti-Mackay structure occurs at N=71 for ρ_0=6. This corresponds to an overlayer which completely covers the five faces surrounding a vertex of the underlying icosahedron. There are smaller peaks at N=58, 61, and 64, which correspond to complete coverage of one, two and three faces, respectively.

Structure 69C has a vertex atom missing from the underlying Mackay icosahedron like 38A. There are also structures (62C, 65D, 72C and 75B) where an atom is added to the surface of the overlayer rather than to the Mackay icosahedron. Again there are transitions between different anti-Mackay structures resulting from small differences in E_{strain}.

The first structure in this size range with a Mackay overlayer is 78D. We expect that the crossover from an anti-Mackay to a Mackay overlayer will again shift to larger size as the range increases, but we have not investigated this prediction in the present work. There are also three icosahedral global minima, 69B, 70C and 71B, which do not fit neatly into either the Mackay or anti-Mackay category. Their surface layers have a Mackay-like character, but are not in correct alignment with the underlying icosahedron. The overlayer has been given a twist about one of the fivefold axis in order to collapse some of the half octahedra at the edge of the overlayer into trigonal bipyramids in a multiple diamond-square-diamond (DSD) process.[77] In fact for M_{71} at ρ_0=5, the lowest energy Mackay structure is a C_{5v} transition state corresponding to a multiple DSD rearrangement between two permutational isomers of 71B.

Fig. 6 illustrates the variation of the icosahedral energies with size. The complete Mackay icosahedra appear as narrow minima separated by broad maxima corresponding to structures with incomplete outer shells. At ρ_0=6 it is only near the top of these maxima that fcc and decahedral structures begin to have similar energies, for example at N=38 and 75.

B. Decahedral clusters

The decahedral global minima are shown in Figs. 11–13. The structures have been grouped according to the number of atoms along the fivefold axis of the pentagonal bipyramid upon which they are based, and the decahedral region of the structural phase diagram (Fig. 4) has also been subdivided on this basis.

Decahedral clusters grow by capping exposed {100} faces and filling in the grooves produced by the reentrant {111} faces. As this process progresses the structure changes from prolate to approximately spherical to oblate. This cycle begins again when a prolate cluster with a longer decahedral axis becomes lower in energy than the oblate cluster (e.g. at $N \approx 30$ and 54). For the clusters based upon a pentagonal bipyramid with 5 atoms along the fivefold axis ($N \geq 54$), the growth proceeds asymmetrically—the decahedral axis does not always pass through the center of the cluster. For example, for 54C the surface structure of the 75-atom Marks decahedron is completed on one side of the cluster before atoms are added to the other.

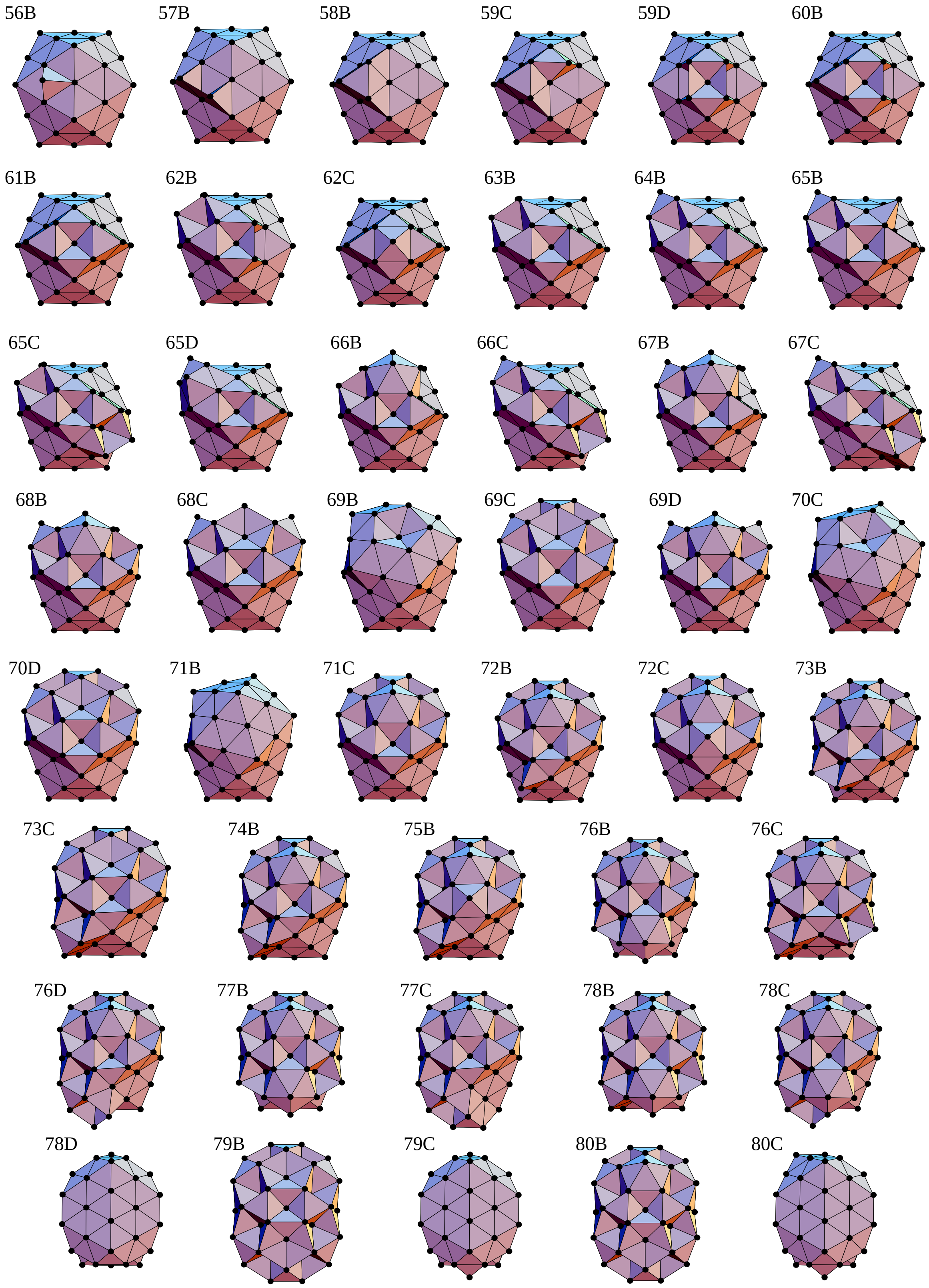

FIG. 10. Icosahedral global minima formed by growth from the 55-atom Mackay icosahedron.

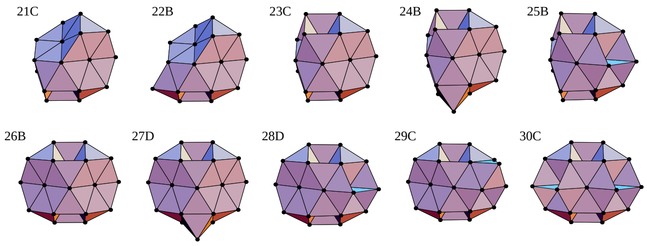

FIG. 11. Global minima based upon a decahedron with three atoms along the fivefold axis.

Deviations from this basic growth scheme occur for N=21–30 (Fig. 11) and N=48–52, 58, 60 and 62 (Fig. 12). These structures are formed by addition of atoms to the {111} faces surrounding the fivefold axis in sites which are hcp with respect to the five fcc tetrahedra that make up the decahedra. These structures are more favourable even though they are more strained than the usual decahedra because they have a larger n_{nn}. For N=21–30 these structures are actually fragments of the 55-atom Mackay icosahedron.

The complete Marks decahedron, 75C, is particularly stable. The value of ρ_0 at which it becomes the global minimum (5.81) is the lowest of any of the decahedra. As this value of ρ_{min} suggests, it is also the global minimum for LJ_{75}.[38] This stability is also indicated by the large peak in $\Delta_2 E$ for ρ_0=10 and 14. Other particularly stable structures occur at N=64 and 71; these are fragments of 75C with 3 and 4 {100} faces of the Marks decahedron complete.

Decahedral structures have been regularly seen in supported metal clusters.[30] However, it is only recently that further experimental evidence for the existence of Marks decahedra has been found in studies of gold clusters passivated by alkylthiolates.[33–35] Whetten and coworkers were able to isolate fractions with narrow size distributions which corresponded to the 75-, 101- and 146-atom Marks decahedra. It is significant to note that our previous paper on Morse clusters[38] foreshadowed this discovery by recognizing the especial stability of the 75-atom Marks decahedron, thus again showing the utility of Morse clusters as a model system.

C. Close-packed clusters

The close-packed global minima are illustrated in Fig. 14. They have a diverse range of structures: there are 4 minima that are fcc, 8 that are hcp and 46 that involve a mixture of stacking sequences and twin planes. The preference for close-packed structures with twin planes, even though at many of the sizes there are fcc isomers with the same number of nearest neighbours, occurs for the same reason that bulk hcp has a lower energy than fcc for pair potentials, namely a larger energetic contribution from next-nearest neighbours. The global minima are broadly based on five structures which are especially stable: the hcp 26C, the truncated octahedron 38D, the tetrahedral 59E and the 'twinned truncated octahedra' 50D and 79F. The latter four give rise to peaks in $\Delta_2 E$ at ρ_0=14 (Fig. 5).

The 38-atom truncated octahedron, 38D, is the most stable fcc cluster in the size range we consider here. It becomes the global minimum at the lowest value of ρ_0 (4.76) of any of the close-packed structures. Curiously, there are two ranges of ρ_0 for which it is the global minimum. At long range, E_{nnn} represents a significant part of the total energy. The truncated octahedron is most stable for $4.76 < \rho_0 < 5.40$ because it is approximately spherical and so has a larger value of E_{nnn} than the more oblate icosahedral structure 38E. For shorter-ranged potentials, the contribution of E_{nnn} diminishes and so 38E becomes the global minimum for $5.40 < \rho_0 < 6.95$ because it has a larger n_{nn}. Then for $\rho_0 > 6.95$ the truncated octahedron again becomes the global minimum because it has a lower strain energy than 38E. There is a growing body of experimental evidence for the importance of truncated octahedra. Parks *et al.* have recently assigned this structure to Ni_{38} by probing the cluster's chemical reactivity.[11] EXAFS (extended x-ray absorption fine structure) spectra of small gold clusters have been interpreted in terms of the presence of truncated octahedral clusters, particularly the 38-atom truncated octahedron.[78] Gold clusters passivated by alkylthiolate molecules selectively form truncated octahedra, which can be isolated and formed into superlattices.[31,32] This structure is also observed for ligated 38-atom platinum clusters.[79]

Structures 50D and 79F both have D_{3h} symmetry and a single twin plane passing through the structure. The two halves of the structure have the surface morphology of truncated octahedra. Indeed 79F can be formed from the 79-atom truncated octahedron by rotation of one half of the structure by 60° about an axis perpendicular to one of the {111} planes. Both structures have the same number of nearest neighbours and 79F is slightly lower in energy only because of the larger contribution from next-nearest neighbours that results from the twin plane. Again there is recent experimental evidence for the stability of this type of structure for gold clusters,[34] although at larger sizes (N=225 and 459) than considered in this study.

The closed-packed structures from N=57–60 are based on 59E. This structure is a 31-atom truncated tetrahedron with the faces covered by four seven-atom hexagonal overlayers occupying hcp sites with respect to the underlying tetrahedron. The stability of 59E comes from the combination of its high proportion of {111} faces and its spherical shape. If atoms are added to one of the grooves in 59E a decahedral-like axis results, indicating a possible path between decahedral and closed-packed clusters.

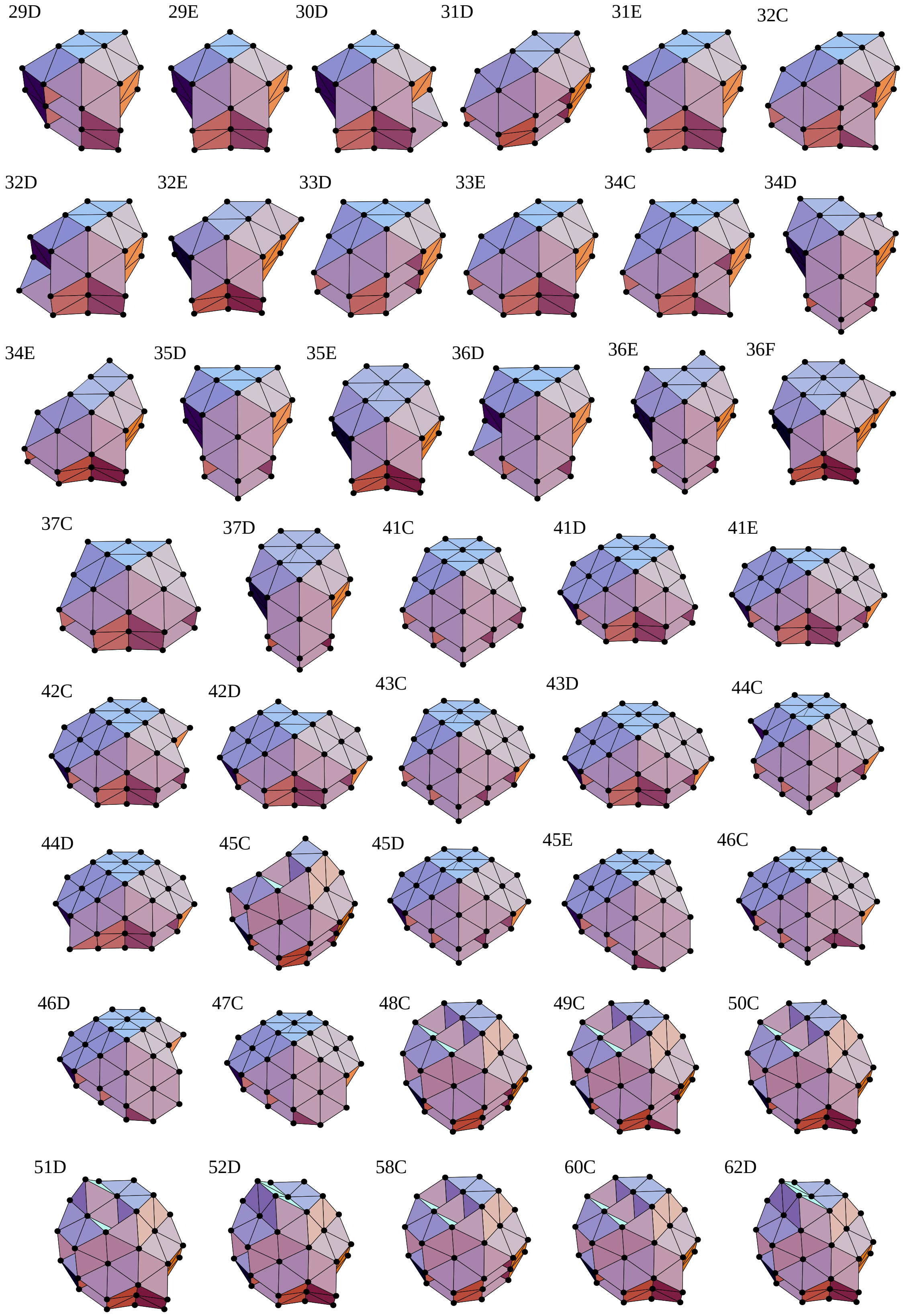

FIG. 12. Global minima based upon a decahedron with four atoms along the fivefold axis.

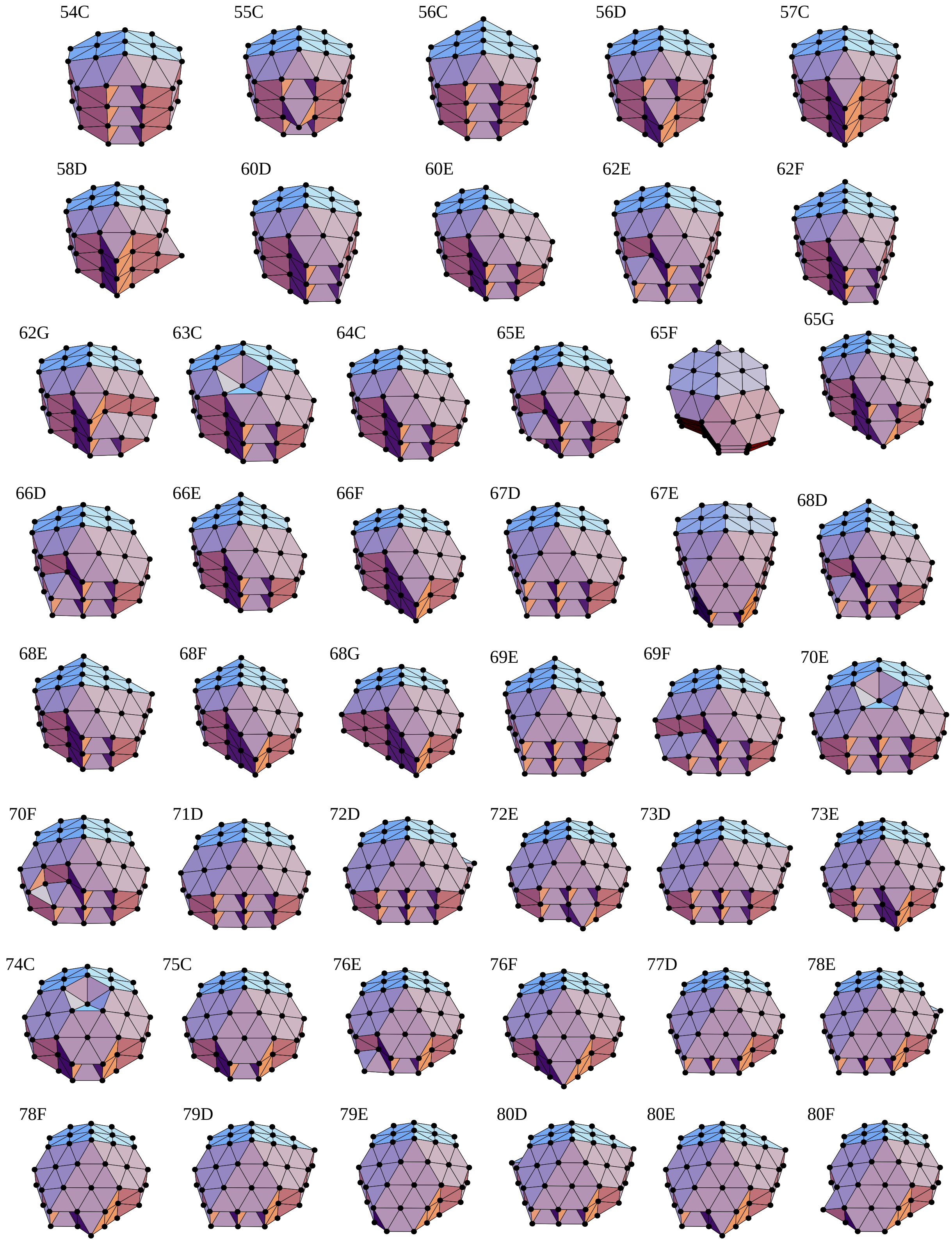

FIG. 13. Global minima based upon a decahedron with five atoms along the fivefold axis.

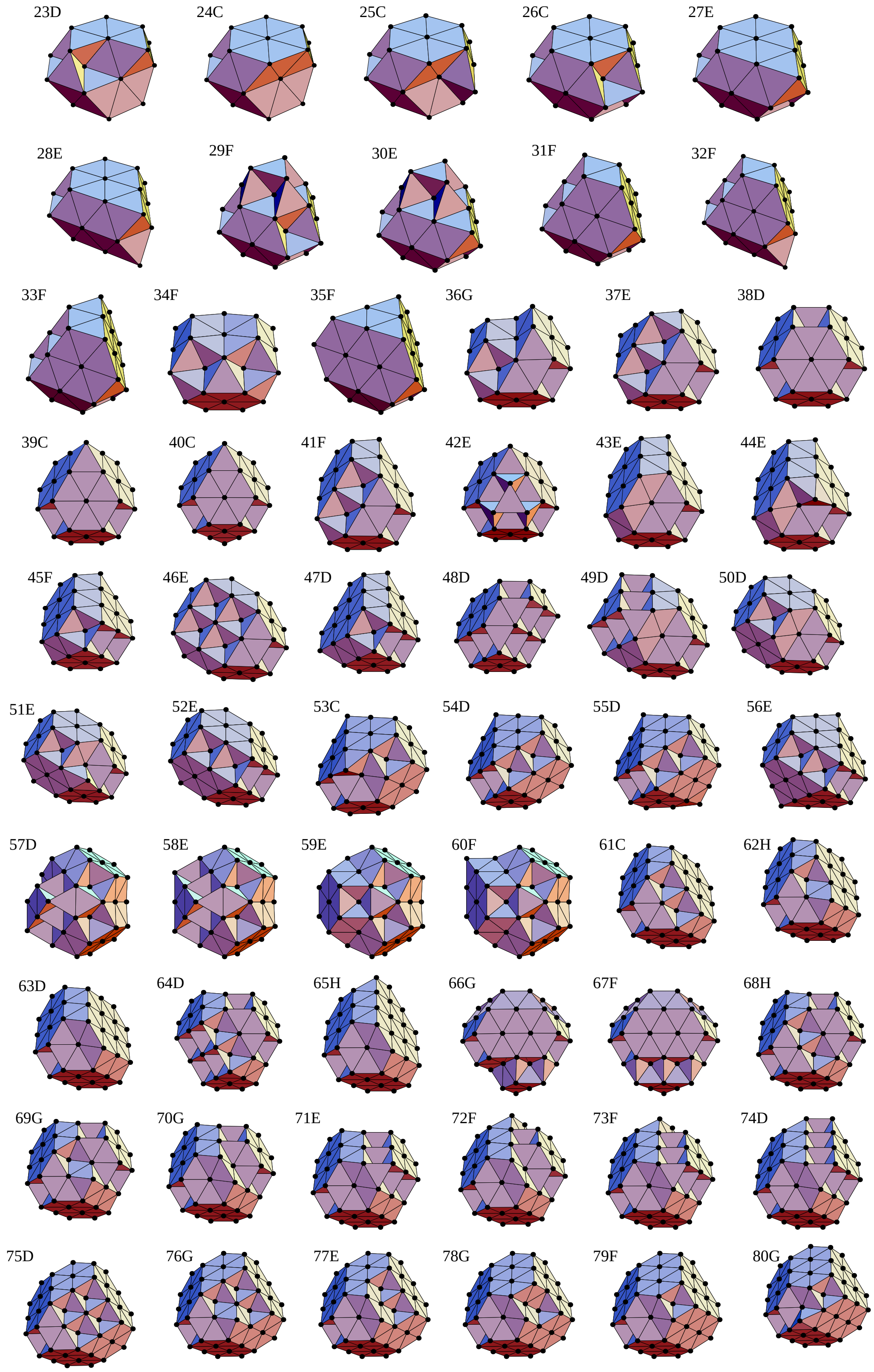

FIG. 14. Global minima based upon close-packing.

It is worth noting that the cuboctahedron is not the lowest energy close-packed structure for N=55. In fact, it has four fewer nearest neighbours than structure 55D. Hence, when magic numbers occur at sizes corresponding to both complete Mackay icosahedra and cuboctahedra[25,26] (N=13, 55, 147, ...) it is more likely that they are due to icosahedra. Furthermore, one has to interpret with caution those studies which seek to find the relative stability of fcc and icosahedral structures by comparing cuboctahedra with Mackay icosahedra[80–83] because the cuboctahedra are likely to be suboptimal fcc structures.

Although this conclusion does not simply carry over to clusters surrounded by ligand shells—the ligands could significantly modify the relative surface energies of {111} and {100} faces—it is interesting to note that a recent reinvestigation of clusters which were originally thought to be cuboctahedral 55-atom gold clusters[84,85] seems to disprove this structural assignment.[86]

D. Structures corresponding to long range

In this subsection, we consider those structures which become the global minimum only at low values of ρ_0. We have restricted our study to those clusters with $\rho_0 \geq 3$, since we do not know of a case where longer-ranged potentials might be relevant. The low ρ_0 structures that we have found separate into two size ranges: those with N around 13 and those with $N > 45$. The former set have been described in a previous paper,[38] but we illustrate them again in Fig. 15 because the connection to Kasper polyhedra[87,88] was not originally identified and because they are important for understanding the structures that occur at larger N.

The majority of the structures associated with low ρ_0 are polytetrahedral: the entire cluster can be divided into tetrahedra with atoms at the vertices. These minima also tend to be close to spherical in shape and highly strained in order to maximize n_{nn}. As we noted earlier, the 13-atom icosahedron is polytetrahedral. In this case, each nearest-neighbour contact between the centre and a vertex is the common edge of five tetrahedra. This is also true of all the nearest-neighbour contacts in the rhombic tricontahedron (45A) which do not lie on the surface. Nearest-neighbour contacts which are surrounded by more or less than five tetrahedra are said to have defects called *disclination lines* running along the interatom vector. Those contacts surrounded by more than five tetrahedra are termed negative disclinations (if there are six it is a $-72°$ disclination, if there are seven a $-144°$ disclination, ...) and those surrounded by fewer than five tetrahedra are termed positive disclinations (if there are four it is a $+72°$ disclination and if there are three a $+144°$ disclination).

Most of the structures associated with low ρ_0 are polytetrahedral and involve disclinations. Although packing five tetrahedra around a nearest-neighbour contact involves some strain, the energetic penalty associated with either more or less tetrahedra is greater. Therefore, structures involving disclinations are only likely to be lowest in energy for long-ranged potentials where the associated strain can be most easily accommodated, and where they must have a larger n_{nn} than the alternative disclination-free structures. A $-72°$ disclination line involves less strain than a $+72°$ disclination line because of the gap that remains when five regular tetrahedra share a common edge (Fig. 3(a)). Consequently, structures which involve only negative disclinations, or an excess of them, are more common amongst the low ρ_0 global minima.

To visualize the network of disclination lines in a structure, one must first partition space according to the Voronoi procedure, in which each point is assigned to the Voronoi polyhedron of the atom to which it is closest. This allows nearest neighbours to be defined as those atoms whose Voronoi polyhedra share a face. The Delaunay network that results from joining all such nearest neighbours is the dual of the Voronoi construction and divides all space into tetrahedra. This definition of a nearest neighbour has been termed geometric, rather than physical (e.g. using a cutoff distance), and the corresponding division of space into tetrahedra is artificial in the sense that it is independent of whether a polytetrahedral description is appropriate.

In practice we determined the Voronoi polyhedra from the fact that a set of four atoms constitutes a Delaunay tetrahedron if the sphere touching all four atoms contains no other atoms.[89] The centre of this sphere is then a vertex of the Voronoi polyhedron of each atom. As the number of tetrahedra around a nearest-neighbour contact is the same as the number of sides for the face common to the Voronoi polyhedra of both nearest neighbours, disclination lines can then be assigned. However, problems can occur in assigning the Delaunay network if there are more than four atoms exactly on the surface of the sphere. Such a degeneracy, which only occurs as a result of symmetry, renders the analysis non-unique. This is the case for the 55-atom Mackay icosahedron and for bulk close-packed solids because of the presence of octahedral interstices, but it is not a problem here since we only apply the method to clusters that are polytetrahedral in character. One further consideration is that the analysis should not be applied to nearest-neighbour contacts between the surface atoms of a cluster.

The smallest global minimum that involves a disclination line is 11A where the central atom is surrounded by a 10-atom coordination shell. This encapsulation gives the structure a larger n_{nn} than the incomplete icosahedron (structure 11B of ref. 38), but results in a larger strain energy.[38] The structure involves a single positive disclination line running through the centre of the cluster. Similarly, for N=12 and 14–16, clusters with a single coordination shell become lower in energy than structures based on the icosahedron at long range. Structures 11A, 12A, 14A, 15A, 16A and 17F (the second lowest energy structure of M_{17} at $\rho_0 = 3$) correspond to Kasper polyhedra. Of these structures 15A is the most stable in terms of the range of ρ_0 for which it is the global minimum.[38] The Kasper polyhedra are the deltahedral coordination shells that involve the minimum number of disclinations. They are important in the Frank-Kasper phases,[87,88] which are crystalline structures that are polytetrahedral and involve ordered arrays of negative disclination lines. Much interest has been focussed on the Frank-Kasper phases because they are closely related to icosahedral quasicrystals.[90] Indeed a recent three-dimensional model of quasicrystalline structure was based upon clusters involving disclination lines similar to those we find here.[91]

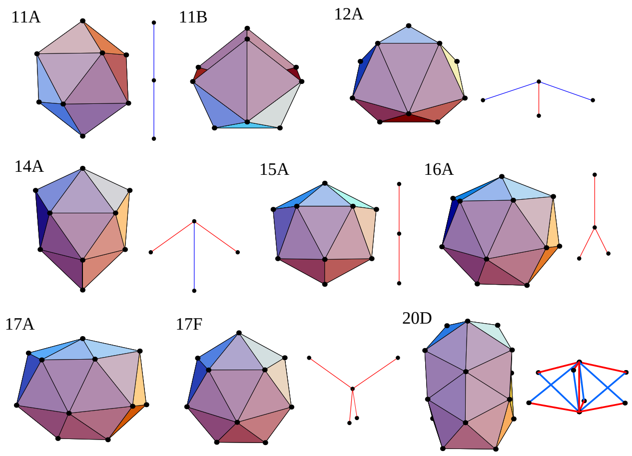

FIG. 15. Low energy minima for small clusters at low values of ρ_0. If appropriate, the disclination network is displayed next to each structure. $-72°$ disclinations are represented by red lines and $+72°$ disclinations by blue lines. 17F and 20C are never global minima.

Structures 11A, 12A, 14A, 15A and 16A are all deltahedral, and so growth can occur in both 'anti-Mackay' and 'Mackay' sites (Fig. 7). However, if one considers the addition of a hexagonal pyramidal cap to the most stable of the Kasper polyhedra, 15A, the result is a D_{6h} structure with a positive disclination running the length of the symmetry axis (a disclinated equivalent of the double icosahedron 19A) which has only the same n_{nn} as the icosahedral structure 22A. Disclinated polytetrahedra cannot compete with the disclination-free polytetrahedral structures produced by an anti-Mackay overlayer on the icosahedron. Only once the latter growth sequence is completed at N=45 are structures with disclinations again global minima (Fig. 16). The one exception is structure 38A, which is similar to the icosahedral structures 38B and 38C, but has two positive disclinations running through the structure in a strange double helical twist.

Interestingly, structures with anti-Mackay growth on 11A have been recently observed for M^+RG_N (M—metal, RG—rare gas) clusters where the metal ion is sufficiently small with respect to the rare gas atoms.[92] The metal ion presumably lies in the centre of the cluster, and the size ratio ensures that the cluster is least strained when the metal ion is surrounded by 10 rare gas atoms. Similarly, one might expect structures with negative disclinations to occur for AB_N clusters when A is sufficiently large with respect to B that a coordination number of larger than twelve is favoured for the A atom.

The most stable disclinated polytetrahedral structures occur at N=53, 57, and 61 (Fig. 5(a)). These are the sizes for which complete 'anti-Mackay' overlayers on 15A, 16A and 17F are possible. The effect of the overlayers is to extend the disclination lines emanating from the central atom. In these structures, those interior atoms not lying on a disclination line are icosahedrally coordinated. Many other minima are related to these stable structures: 51A and 52A are based on 53A but with missing vertex atoms; similarly, 59B and 60A are based on 61A; and 70A and 74A are based on 57A and 61A, respectively, but with an additional 13-atom cap which extends one of the 'arms' of the disclination network. Furthermore, many of the other structures include parts of the disclination networks of 53A, 57A and 61A, but combined with a more disordered array of disclinations in another part of the cluster.

Other interesting structures are also seen. 47A, 50A and 59A seem to have a mixture of Mackay and anti-Mackay overlayers. 64A is formed from the rhombic tricontahedron 45A by the extension of the structure along a three-fold axis and the addition of a ring of atoms in the centre. In the middle of 64A is the D_{3d} structure 20D (the third lowest energy structure for M_{20} at ρ_0=3) which can be regarded as two highly strained interpenetrating icosahedra. However, for the larger clusters it becomes difficult to recognize any structural motifs, and some just seem to be disordered tangles of disclinations.

The above results are particularly interesting because of their relevance to our understanding of liquid structure. The minima described above, when reoptimized at larger values of ρ_0, correlate with structures which lie in the lower energy range of the band of minima associated with liquid-like clusters.[41,42] This is because simple liquids have significant polytetrahedral character,[93] as has been shown by the success of the dense random packing of hard spheres[94,95] as a model for metallic glasses[96] and later by computer simulations.[97] Indeed, Nelson has suggested that simple liquids are polytetrahedral packings that are characterized by a disordered arrangement of disclination lines.[98,99] Consequently, by examining the global minima associated with low ρ_0 we can study the size evolution of polytetrahedral packings, and the development of bulk liquid structure.

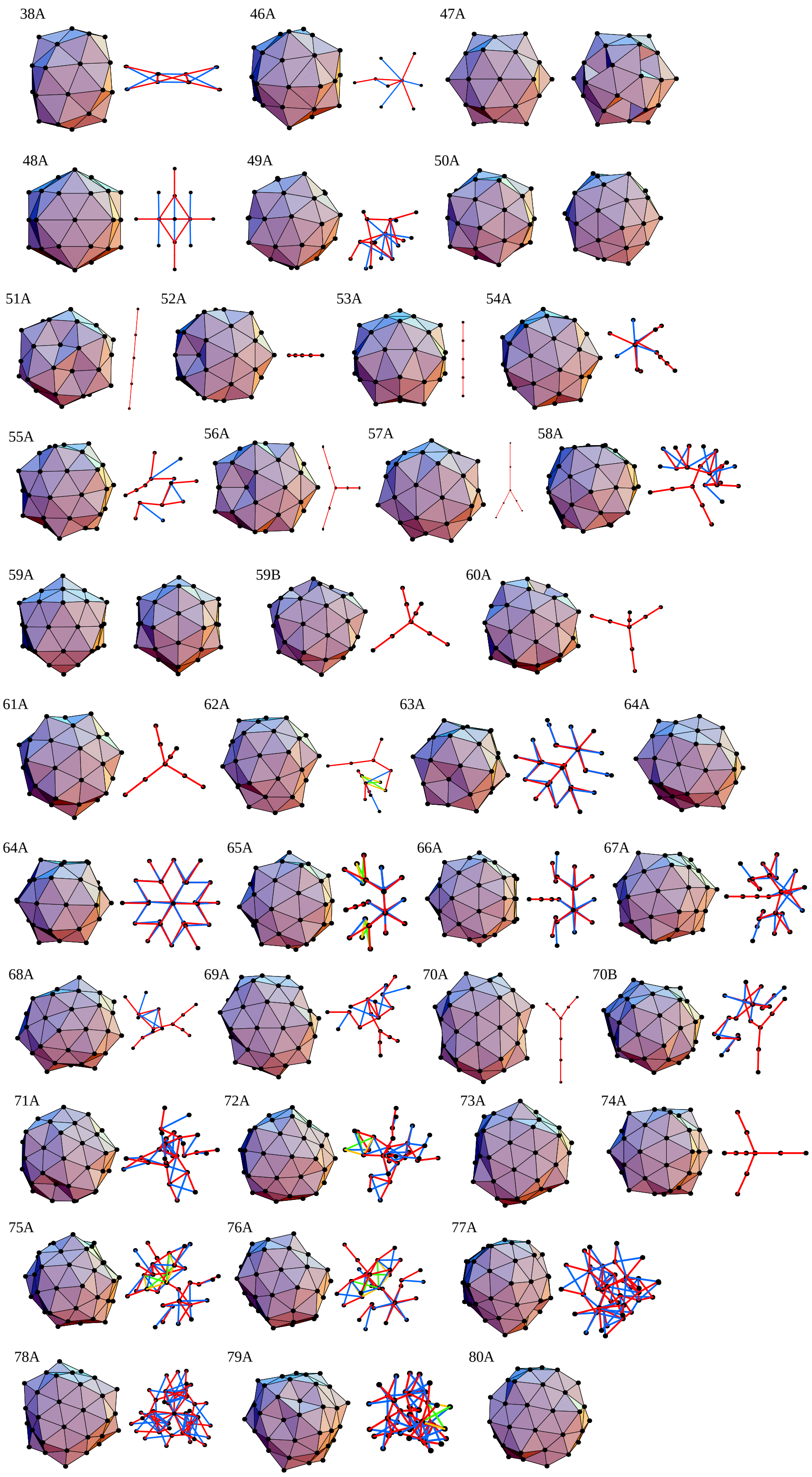

FIG. 16. Global minima at low values of ρ_0 for $N \geq 38$. If appropriate, the disclination network is displayed next to each structure. -72° disclinations are represented by red lines, $+72^\circ$ disclinations by blue lines, -144° disclinations by green lines and $+144^\circ$ disclinations by yellow lines.

At small sizes disclination-free polytetrahedra based on icosahedra with anti-Mackay overlayers are possible; at larger sizes polytetrahedra with ordered arrangements of disclinations are most common, and finally at the largest sizes in this study the polytetrahedra have a disordered disclination network. The latter geometries are structurally very similar to fragments of bulk liquid, except that the density of disclination lines is lower.[42]

Theoretical studies of sodium clusters have shown that amorphous structures are lower in energy than regular geometries up to at least 340 atoms, the largest size considered in that study.[100] The present results suggest that the these disordered structures are due to the relatively long range of the sodium interatomic potential. Amorphous structure for sodium is also suggested by the experimental observation of electronic shells[101] and supershells,[102] which are incompatible with any of the ordered morphologies one might expect.[103] Indeed, the transition from electronic to geometric magic numbers which occurs at about 1000 atoms[25] probably reflects a change in the lowest energy structures from amorphous minima to Mackay icosahedra, which can be explained by the twin effects of the size and the range of the potential.[41,42]

Since most minima associated with small values of ρ_0 do not have a common lattice or packing scheme, it is difficult to predict the low energy structures, and so most have been found by one of the global optimization methods. Fortunately, these methods are most likely to succeed for long range potentials because the corresponding PES's are smoother and support fewer minima than for shorter range. Another consequence of the lack of lattice structure is that the differentiation between nearest neighbours and next-nearest neighbours becomes ambiguous and the decomposition of eqn. (2) more arbitrary. For these clusters we chose to define n_{nn} using a cutoff at ρ_0=4 which corresponds to the distance at which the pair energy is $0.6\,\epsilon$.

IV. DISCUSSION

In this paper we have attempted to find the global minima for Morse clusters as a function of ρ_0 and the number of atoms. The global potential energy minimum represents the equilibrium structure at zero Kelvin, but to predict the structure at non-zero temperatures we must consider the free energy, and the effect of other low energy minima. This can be done by summing the density of states over all the relevant minima.[104] An illustration of this approach for understanding the structure of Morse clusters has been given previously,[38,105] revealing that for M_{75} at ρ_0=6, the equilibrium structure changed from decahedral to icosahedral at very low temperature. This transition is simply a consequence of the larger entropy for the icosahedral region of configuration space—there are far more low energy icosahedral minima.

This effect is likely to be general. At the magic numbers for a morphology the entropy will be low because there is a single unique low entropy structure and a large gap to other isomers with the same morphology. Therefore the finite temperature equivalent of the structural phase diagram of Fig. 4 is likely to show weakened magic number effects and so have smoother boundaries between the different morphologies. Furthermore, the energy gap between the lowest energy ordered minimum and the liquid-like band of minima increases as the range becomes shorter, and hence the melting temperature increases with ρ_0.[42] Therefore the region of the phase diagram where disordered polytetrahedral structures have the lowest free energy is likely to spread up from the bottom as the temperature increases.

In this paper we have considered only isotropic pairwise additive interactions. As noble gas clusters and clusters of C_{60} molecules can be reasonably modelled by such potentials we would expect the structures we have found at the appropriate values of ρ_0 to be similar to the actual structures of these clusters. Our results lead us to predict that neutral clusters of C_{60} molecules exhibit decahedral and fcc structures at small sizes because of the short range of the intermolecular potential. This basic conclusion has been confirmed in studies using more realistic potentials.[72,106]

In contrast, making predictions for metal clusters is problematic because the range of the potential is only one factor determining the structure and many-body terms, in particular, may also be important.[107,108] These terms may affect the relative surface energies of {111} and {100} faces, and so alter the energetic competition between icosahedral, decahedral and fcc structures.[81] For example, in a study of lead clusters cuboctahedra are always found to be lower in energy than icosahedra because the surface energies of {111} and {100} faces are nearly equal.[83]

Nevertheless our results are of value to the field of metal cluster structure. Firstly, they enable particularly stable structural forms to be identified. For example, in our previous paper on Morse clusters we identified the 38-atom octahedron and the 75-atom Marks decahedron as particularly stable. Subsequently, they have both been observed experimentally;[11,33,35] it even being possible to isolate fractions of the latter when passivated by surfactants. This correspondence between the Morse structures and those of real systems encourages us to believe that some of the general principles that determine stability in our simple model system do carry over to real clusters.

Secondly, the Morse structural database should be useful in providing candidate structures for comparison with the indirect structural information yielded by experiments on size-selected clusters. Finally, the database can also provide plausible starting structures for theoretical studies with more realistic, but computationally expensive, descriptions of the interactions; this expense would prevent the type of extensive searches that have been performed in this paper. Indeed, we have used the database in this way in studies of metal clusters modelled by the

Sutton-Chen family of potentials[20] and clusters of C_{60} molecules.[72,106] For these reasons, the coordinates for all the global minima given in this and previous papers[38,43] will be made available on the world-wide-web.[109]

V. CONCLUSION

We have shown how the range of an isotropic pairwise additive potential determines the structure of atomic clusters. In particular, we have identified four principal structural regimes. For long-ranged potentials at sizes $N = 10$–18 and $N > 45$ the global minima are generally polytetrahedral and can be analyzed in terms of disclination lines. For the smaller clusters the disclinations form ordered arrangements and the structures are fragments of bulk Frank-Kasper phases. As the size increases it becomes more likely that the disclination network is a disordered tangle; these global minima have amorphous structures similar to those exhibited by liquid-like clusters. At intermediate ranges of the potential icosahedra are dominant. As the range decreases, first decahedral and then fcc structures become lowest in energy. These trends have been explained by considering the strain energies and the number of nearest neighbour contacts associated with each regime. The effect of decreasing the range of the potential is to destabilize the strained structures.

ACKNOWLEDGMENTS

We are grateful to the Engineering and Physical Sciences Research Council (J.P.K.D.) and the Royal Society (D.J.W.) for financial support.

TABLE I. Global minima of M_N for $N \leq 80$. Energies at values of ρ_0 for which the structure is the global minimum are given in bold. ρ_{min} and ρ_{max} give the range of ρ_o for which the structure is the global minimum. If at a particular value of ρ_0 a structure is not a minimum but a higher order saddle point, the index of the stationary point (the number of negative eigenvalues of the Hessian) is given in square brackets after the energy. E_{strain} has been calculated at ρ_0=10. If a structure is not stable at ρ_0=10 no value of E_{strain} is given. All energies are given in ϵ.

	PG	n_{nn}	E_{strain}	$\rho_0 = 3$	$\rho_0 = 6$	$\rho_0 = 10$	$\rho_0 = 14$	ρ_{min}	ρ_{max}
5A	D_{3h}	9	0.000	**-9.299500**	**-9.044930**	**-9.003565**	**-9.000283**		
6A	O_h	12	0.000	**-13.544229**	**-12.487810**	**-12.094943**	**-12.018170**		
7A	D_{5h}	16	0.062	**-17.552961**	**-16.207580**	**-15.956512**	**-15.883113**		
8A	D_{2d}	18	0.006	**-22.042901**	-19.161862	-18.275118	-18.076248		5.28
8B	C_s	19	0.062		**-19.327420**	**-18.964638**	**-18.883688**	5.28	
9A	D_{3h}	21	0.002	**-26.778449**	-22.330837	-21.213531	-21.037957		3.42
9B	C_{2v}	23	0.186	-26.607698	**-23.417190**	**-22.850758**	**-22.644892**	3.42	
10A	D_{4d}	24	0.002	-31.519768	-25.503904	-24.204958	-24.031994		2.28
10B	C_{3v}	27	0.694	**-31.888630**	**-27.473283**	**-26.583857**	**-26.132735**	2.28	
11A	D_{4d}	34	10.374	**-37.930817**	-28.795153[4]	-23.666072[5]			3.40
11B	C_{2v}	32		-37.891674[1]				3.40	3.67
11C	C_{2v}	31	0.792		**-31.521880**	**-30.265230**	-29.588130[1]	3.67	13.57
11D	C_s	30					**-29.596054**	13.57	15.29
11E	C_2	30	0.248	-36.613190[1]	-30.698890	-29.808994	-29.524398	15.29	20.60
11F	C_{2v}	29	0.001	-36.697760	-30.431713	-29.215510	-29.037941	20.60	
12A	C_{2v}	38		-43.971339[1]	-35.199881[1]				2.63
12B	C_{5v}	36	1.704	**-44.097880**	**-36.400278**	**-34.366755**	-33.115942[1]	2.63	12.15
12C	C_s	34					-33.199505	12.15	13.03
12D	D_{2d}	34	0.346	-41.816393	-34.838761	-33.724155	**-33.332305**	13.03	17.08
12E	D_{3h}	33	0.001	-42.121440	-34.568002	-33.222331	-33.038298	17.08	
13A	I_h	42	2.425	**-51.737046**	**-42.439863**	**-39.662975**	**-37.258877**		14.76
13B	D_{5h}	37	0.141	-49.998058[1]	-39.360710[1]	-37.208019[1]	-36.790507	14.76	
14A	C_{2v}	46	4.373	**-56.754744**	-44.827522[1]	-41.717043[1]			3.23
14B	C_{3v}	45	2.425	-56.660471	**-45.619277**	**-42.675222**	-40.259823	3.23	13.06
14C	C_{2v}	41	0.141	-55.971620[2]	-43.634048[1]	-41.249282	**-40.798348**	13.06	
15A	D_{6d}	50	9.527	**-63.162119**	-47.570579	-40.569211[10]	-35.758904[13]		3.72
15B	C_{2v}	49	2.573	-62.593904	**-49.748409**	**-46.541404**	-44.086633	3.72	12.71
15C	C_{2v}	45	0.141	-62.631372[2]	-47.952559	-45.293844	**-44.806437**	12.71	
16A	D_{3h}	54	11.222	**-69.140648**	-50.834213	-42.887569[12]			3.39
16B	C_s	53	2.868	-68.757203	**-53.845835**	**-50.261947**	-47.831957	3.39	11.99
16C	C_{2v}	49	0.142	-68.575718[1]	-52.265348	-49.338173	**-48.814517**	11.99	

TABLE I. continued.

	PG	n_{nn}	E_{strain}	$\rho_0 = 3$	$\rho_0 = 6$	$\rho_0 = 10$	$\rho_0 = 14$	ρ_{min}	ρ_{max}
17A	D_{3h}	58		**-75.662417**	-53.156042[2]				3.42
17B	C_{3v}	57	3.372	-75.147372	-57.884517	-53.772213	-51.329560	3.42	4.88
17C	C_s	57	3.281	-75.091367	-57.912963	-53.862044	-51.440588	4.88	4.91
17D	C_2	57	3.163	-75.005403	**-57.941386**	**-53.983559**		4.91	11.30
17E	C_{2v}	53	0.142	-74.868921[1]	-56.573571	-53.382277	**-52.822588**	11.30	
18A	C_2	65		**-82.579266**	-59.881449[1]			2.14	3.03
18B	C_{5v}	62	4.500	-82.548885	**-62.689245**	**-57.657135**	-54.059707	3.03	10.13
18C	C_s	61	3.528	-81.256639	-62.002920	-57.634324	-55.776126	10.13	10.43
18D	D_{5h}	57	0.142	-81.490185	-60.926500	-57.429683	**-56.830907**	10.43	
19A	D_{5h}	68	6.001	**-90.647461**	**-68.492285**	**-62.166843**	-56.676685[4]		10.70
19B	C_{2v}	61	0.151	-87.485744	-65.064771	-61.427105	**-60.812425**	10.70	
20A	C_{2v}	72	6.507	**-97.417393**	**-72.507782**	**-65.679115**	-61.327229	2.02	10.24
20B	C_{2v}	65	0.162	-94.222416	-69.202704	-65.423697	**-64.791953**	10.24	
21A	C_{2v}	76	7.133	**-104.336946**	-76.487266	-69.068687	-65.179591[1]		5.40
21B	C_1	76	6.922	-104.004129	**-76.529139**	-69.276346	-65.778898	5.40	9.84
21C	C_s	69	0.169		-73.577014	**-69.449904**	**-68.783571**	9.84	
22A	C_s	81	8.198	**-112.041223**	**-81.136735**	-73.014321	-68.580862[1]		9.58
22B	C_1	73	0.169		-77.887855	**-73.494292**	**-72.791747**	9.58	
23A	D_{3h}	87	10.597	**-120.786879**	**-86.735494**	-76.630624	-70.816059[5]		8.35
23B	D_{3h}	84	6.097	-116.279438	-84.940552	-78.143867	-74.442341[2]	8.35	9.71
23C	C_s	78	0.433		-83.504908	**-78.325380**	**-77.302495**	9.71	22.45
23D	C_1	76	0.007		-82.252747	-76.898804	-76.157457	22.45	
24A	C_s	91	10.947	**-127.884549**	**-90.685398**	-80.295459[1]	-74.613738[2]	2.79	8.55
24B	C_1	82	0.434		-87.820376	**-82.370214**	**-81.309508**	8.55	15.34
24C	C_{2v}	81	0.007		-87.626843	-81.941420	-81.164168	15.34	
25A	C_s	96	12.090	**-136.072704**	**-95.127899**	-84.168765		2.62	7.76
25B	C_{3v}	87	0.893		-93.342771	**-86.989688**	**-85.477376**	7.76	15.40
25C	C_s	85	0.010		-92.241466	-86.015371	-85.176789	15.40	
26A	T_d	102	15.393	**-145.322134**	**-100.549598**	-86.882333[11]			7.89
26B	C_{2v}	91	0.491	-138.940920[3]	-97.363225	**-91.370250**	**-90.210764**	7.89	14.20
26C	D_{3h}	90	0.008		-97.648652	-91.085136	-90.189274	14.20	
27A	C_s	106		**-152.513867**	-104.489430				4.72
27B	C_{2v}	106		-151.734925	**-104.745275**			4.72	7.71
27C	C_s	97	3.076		-102.749592	-94.736230	-91.236563[1]	7.71	8.53
27D	C_s	95	0.491	-146.171281[2]	-101.722918	**-95.419490**	**-94.219798**	8.53	14.22
27E	C_s	94	0.008		-101.920210	-95.121297	-94.195553	14.22	
28A	C_s	111		**-160.773356**	-108.854564				4.82
28B	C_s	111		-160.385239	**-108.997831**			4.82	6.70
28C	C_{3v}	102	3.369		-108.186446	-99.524026	-95.692056	6.70	8.88
28D	C_s	100	0.983		-107.213896	**-100.008358**	**-98.331711**	8.88	14.57
28E	C_{2v}	98	0.008		-106.238844	-99.161073	-98.202117	14.57	
29A	D_{3h}	117		**-170.115560**	**-114.145949**				6.90
29B	C_1	106	3.370		-112.655980	-103.586316	-99.702681	6.90	8.95
29C	C_1	104	0.988		-111.543685	**-104.051412**	-102.333194	8.95	11.07
29D	C_{2v}	103	0.246		-111.508961	-103.946446	-102.743899	11.07	11.17
29E	D_{5h}	103	0.225	-164.720567	-111.353973	-103.926827	**-102.774589**	11.17	21.90
29F	C_{3v}	102	0.010		-111.135014[1]	-103.298583	-102.227015	21.90	
30A	C_{2v}	121		**-177.578647**	-118.115802				4.47
30B	C_{2v}	121	8.279	-176.940971	**-118.432844**	-103.407917[1]		4.47	6.86
30C	C_{2v}	109	1.538		-117.010672	**-108.571179**	-106.426033	6.86	12.61
30D	C_s	107	0.238		-115.940968	-107.985497	**-106.765372**	12.61	21.33
30E	C_s	106	0.012		-115.625207	-107.367696	-106.239394	21.33	

TABLE I. continued.

	PG	n_{nn}	E_{strain}	$\rho_0 = 3$	$\rho_0 = 6$	$\rho_0 = 10$	$\rho_0 = 14$	ρ_{min}	ρ_{max}
31A	C_1	126		**-185.984248**	-122.440052				4.60
31B	C_s	126		-185.299446	**-122.857743**			4.60	6.35
31C	C_s	115	3.490		-122.342421	-112.542723	-108.722594	6.35	8.93
31D	C_{2v}	112	0.269	-184.500261	-121.523693	**-113.066115**	-111.724317	8.93	10.98
31E	C_{2v}	112	0.246	-181.901112[1]	-121.367441	-113.048378	**-111.760670**	10.98	20.90
31F	C_s	111	0.011		-120.805231	-112.376045	-111.239641	20.90	
32A	C_{2v}	132		**-195.468461**	-127.643751				5.93
32B	C_{2v}	120	3.831		**-127.771395**	**-117.284334**		5.93	10.27
32C	C_s	116	0.269		-125.953587	-117.116756	-115.732921	10.27	11.33
32D	C_1	116	0.260		-125.950348	-117.105640	-115.748493	11.33	11.40
32E	C_s	116	0.246	-188.807956[1]	-125.644966	-117.086755	**-115.767561**	11.40	20.90
32F	C_s	115	0.011		-125.126341	-116.415892	-115.246208	20.90	
33A	C_s	137		**-204.208737**	-131.704206[1]				5.35
33B	C_{5v}	137		-203.575130	-131.773513			5.35	5.74
33C	C_s	124	3.832		**-132.287431**	-121.352047		5.74	8.46
33D	C_{2v}	121	0.313		-131.555811	-122.160387	-120.665738	8.46	9.71
33E	C_{2v}	121	0.269		-131.378662	**-122.167479**	**-120.741345**	9.71	19.88
33F	C_s	120	0.011		-130.466899	-121.454645	-120.252542	19.88	
34A	D_{5h}	143		**-214.068392**	-136.468311				5.87
34B	C_{2v}	128	3.832	-209.946801	**-136.797544**	-125.419532		5.87	8.52
34C	C_s	125	0.313		-135.989024	-126.211991	-124.674640	8.52	9.55
34D	C_1	125	0.289		-135.963257	**-126.217685**	-124.717107	9.55	10.72
34E	C_s	125	0.269	-206.153688[2]	-135.656902	-126.205973	**-124.748271**	10.72	19.86
34F	C_{2v}	124	0.013		-135.532334	-125.625477	-124.283737	19.86	
35A	C_s	147		**-221.771452**	-140.503355				4.05
35B	C_{3v}	147		-221.293580	-141.106305			4.05	5.62
35C	C_1	133	3.975		**-141.957188**	-130.282153	-126.119817	5.62	8.08
35D	C_{2v}	130	0.304		-141.402997	**-131.274427**	-129.699893	8.08	11.46
35E	C_{2v}	130	0.279	-215.495670[2]	-141.051852	-131.239157	**-129.737360**	11.46	19.59
35F	C_{3v}	129	0.011		-140.132124	-130.533259	-129.265442	19.59	
36A	C_s	152		**-230.508264**	-144.827464				4.68
36B	C_1	152		-229.689435	-145.273702			4.68	5.07
36C	C_s	138	4.351		**-147.381965**	-134.989116		5.07	9.51
36D	C_1	134	0.334		-145.984498	-135.312738	-133.656022	9.51	9.86
36E	C_s	134	0.303		-145.732293	**-135.315392**	-133.706961	9.86	11.41
36F	C_s	134	0.280	-222.900558[1]	-145.378315	-135.281551	**-133.744666**	11.41	19.56
36G	C_s	133	0.015		-145.649065	-134.766521	-133.308212	19.56	
37A	C_s	158		**-240.008130**	-149.765993				5.25
37B	C_1	142	4.352		**-151.891203**	-139.055858	-134.764790	5.25	7.62
37C	C_{2v}	139	0.357		-151.435570	**-140.360228**	-138.622227	7.62	10.17
37D	C_{2v}	139	0.306	-233.080175[3]	-151.061897	-140.354330	**-138.708582**	10.17	18.49
37E	C_{3v}	138	0.015		-151.100849	-139.837570	-138.320817	18.49	
38A	D_2	164	30.138	**-249.159174**	-153.208710[3]	-134.319674[3]			3.15
38B	C_1	163	27.962	-249.087740	-154.165069	-135.519468	-129.339213	3.15	4.70
38C	C_s	163		-248.600369	-154.041575			4.70	4.76
38D	O_h	144	0.013	-246.414723[4]	-157.406902	**-145.849817**	**-144.321054**	4.76	5.40
								6.95	
38E	C_{5v}	147	3.714		**-157.477108**	-144.756555		5.40	6.95
39A	C_{2v}	169		**-258.944962**	-158.266473				4.48
39B	C_{5v}	153	5.039		**-163.481990**	-149.455758		4.48	9.46
39C	C_{4v}	148	0.014		-161.701728	**-149.887173**	**-148.327400**	9.46	
40A	C_s	174		**-268.394773**	-163.956596				4.51
40B	C_s	157	5.040	-263.925318	**-167.993097**	-153.524033	-148.492778[1]	4.51	9.51
40C	D_{4h}	152	0.014	-261.115599[3]	-165.996196	**-153.924517**	**-152.333745**	9.51	
41A	C_{2v}	180		**-278.405573**					4.60
41B	C_s	161	5.040	-273.699508[1]	**-172.526828**	-157.593200		4.60	8.75

TABLE I. continued

	PG	n_{nn}	E_{strain}	$\rho_0 = 3$	$\rho_0 = 6$	$\rho_0 = 10$	$\rho_0 = 14$	ρ_{min}	ρ_{max}
41C	C_{2v}	157	0.435		-171.124667	-158.505557	-156.511959	8.75	9.60
41D	C_s	157	0.368	-269.034859[4]	-170.808262	**-158.520688**	-156.630647	9.60	11.06
41E	C_{2v}	157	0.366	-267.688391[4]	-170.758682	-158.518482	**-156.633479**	11.06	16.83
41F	C_s	156	0.017		-170.902496	-158.066916	-156.359354	16.83	
42A	C_{3v}	186		**-288.335415**	-172.252388[1]				4.54
42B	C_s	166	5.275	-282.296210[1]	**-177.680222**	-162.365546	-157.124535	4.54	9.77
42C	C_s	161	0.368		-175.184389	**-162.565848**	-160.638215	9.77	11.10
42D	C_s	161	0.367		-175.135897	-162.563540	**-160.641020**	11.10	16.82
42E	C_s	160	0.017		-175.405455	-162.133633	-160.371244	16.82	
43A	C_{2v}	192		**-298.172449**	-175.540353[2]				4.40
43B	C_s	171		-290.632163[2]	**-183.092699**			4.40	9.34
43C	C_{2v}	166	0.443		-180.837781	-167.585928	-165.511347	9.34	9.57
43D	C_{2v}	166	0.374	-288.301568[2]	-180.515098	**-167.602632**	**-165.634973**	9.57	16.66
43E	C_1	165	0.017		-180.662511	-167.152124	-165.372773	16.66	
44A	C_{5v}	198		**-308.277011**	-179.032310[8]				4.38
44B	C_1	175	5.722	-302.003640	**-187.626292**	-171.071131	-165.689737	4.38	9.38
44C	C_s	170	0.443		-185.214201	-171.631403	-169.519034	9.38	9.65
44D	C_s	170	0.374	-300.113694[3]	-184.841212	**-171.645465**	**-169.642441**	9.65	16.65
44E	C_1	169	0.020		-185.296321	-171.226450	-169.385406	16.65	
45A	I_h	204		**-318.660653**	-182.301077[24]				4.24
45B	C_1	180	5.965	-310.750385	**-192.954739**	-175.389424	-169.712668	4.24	8.72
45C	C_s	175	0.691		-191.230983	-176.548074	-174.095718	8.72	8.95
45D	C_{2v}	175	0.452		-190.548331	**-176.665997**	-174.510080	8.95	11.79
45E	C_{2v}	175	0.451	-303.604189[3]	-190.500098	-176.663202	**-174.511633**	11.79	15.03
45F	C_s	174	0.018		-190.708793	-176.296327	-174.397893	15.03	
46A	C_s	207		**-327.033118**					3.96
46B	C_{2v}	186	6.646	-320.118738[1]	**-199.177751**	**-181.236182**	-174.605103[1]	3.96	10.46
46C	C_s	179	0.452		-194.923850	-180.711434	-178.517769	10.46	11.79
46D	C_s	179	0.451		-194.876995	-180.708654	**-178.519320**	11.79	14.97
46E	C_s	178	0.019		-195.426416	-180.401063	-178.416567	14.97	
47A	C_3	210	40.212	**-336.666189**	-194.242255	-170.368382			4.03
47B	C_1	190	6.648	-331.591008	**-203.704178**	-185.301500	-178.621197	4.03	9.60
47C	C_{2v}	184	0.461	-323.010894[6]	-200.256505	**-185.745782**	**-183.508227**	9.60	14.86
47D	C_s	183	0.019		-200.473614	-185.381591	-183.411312	14.86	
48A	C_{2v}	213		**-346.662788**					4.01
48B	C_s	195	7.464	-340.395646[1]	**-209.044000**	-189.5566723	-182.617917[1]	4.01	8.01
48C	C_{2v}	190	0.808		-207.541529	**-191.586299**	**-188.888965**	8.01	20.22
48D	C_s	187	0.020		-205.418604	-189.535478	-187.440413	20.22	
49A	C_s	219		**-356.412817**					3.91
49B	C_{3v}	201	7.770	-350.540378[1]	**-215.253702**	-195.275059	-187.212009	3.91	9.70
49C	C_s	194	0.808		-211.978083	**-195.639320**	**-192.898412**	9.70	16.14
49D	C_{3v}	192	0.021		-211.117300	-194.627748	-192.455390	16.14	
50A	C_{5v}	224		**-366.635589**					4.04
50B	C_s	205	7.770		**-219.820229**	-199.344795	-191.239955	4.04	8.85
50C	C_s	199	0.809	-360.600022[2]	-217.406110	**-200.691615**	-197.906988	8.85	10.50
50D	D_{3h}	198	0.020		-217.432647	-200.640183	**-198.455633**	10.50	
51A	C_2	232		**-376.673413**	-217.627962				3.74
51B	C_{2v}	210	9.360	-373.932555[1]	**-225.391240**	-202.911593		3.74	6.59
51C	C_s	210	8.551	-374.031668[1]	-225.236760	-203.643178	-195.286917	6.59	9.18
51D	C_s	203	0.809		-221.842387	**-204.744598**	-201.916433	9.18	10.33
51E	C_s	202	0.023		-222.080140	-204.714809	**-202.468274**	10.33	
52A	C_s	238		**-387.587332**					3.71
52B	C_{3v}	216	9.618	-384.520749	**-231.615013**	-208.673261	-199.353198	3.71	6.61
52C	C_{2v}	216	8.840		-231.443769	-209.379230	-199.715952	6.61	9.72
52D	C_{2v}	208	0.809	-380.031663[3]	-227.268275	**-209.796728**	-206.924957	9.72	10.15
52E	C_{2v}	207	0.022		-227.500884	-209.784832	**-207.480764**	10.15	

TABLE I. continued

	PG	n_{nn}	E_{strain}	$\rho_0 = 3$	$\rho_0 = 6$	$\rho_0 = 10$	$\rho_0 = 14$	ρ_{min}	ρ_{max}
53A	D_{6d}	244		**-398.783184**					3.70
53B	C_{2v}	222	9.902	-395.150063	**-237.834976**	**-214.409721**	-203.180586[1]	3.70	10.30
53C	C_s	211	0.025		-232.147467	-213.859451	**-211.493405**	10.30	
54A	C_s	248		**-407.966010**	-232.987285				3.41
54B	C_{5v}	228	10.215	-405.831836	**-244.058174**	**-220.118611**	-208.329991	3.41	10.32
54C	C_{2v}	217	0.465		-238.114592	-219.426691	**-216.636864**	10.32	15.10
54D	C_{2v}	216	0.024		-237.568575	-218.929453	-216.505895	15.10	
55A	C_1	252		**-417.918562**					3.25
55B	I_h	234	10.543	-416.625645	**-250.286609**	**-225.814286**	-213.523774	3.25	11.15
55C	C_{2v}	221	0.465		-242.622450	-223.482018	**-220.646208**	11.15	15.09
55D	C_s	220	0.027		-242.211381	-223.003991	-220.518533	15.09	
56A	C_s	258		**-428.611289**					3.60
56B	C_{3v}	237	10.545	-425.709433	**-253.922955**	**-228.900154**	-216.537609	3.60	10.18
56C	C_{2v}	226	0.481		-248.167730	-228.552734	-225.633470	10.18	11.38
56D	C_s	226	0.465		-248.051289	-228.533805	**-225.655136**	11.38	15.07
56E	D_{3h}	225	0.026		-247.635625	-228.074040	-225.531024	15.07	
57A	D_{3h}	264		**-439.960320**					4.13
57B	C_s	241	10.563	-436.124573[1]	**-258.041717**	-232.877539	-220.502856	4.13	9.61
57C	C_{2v}	231	0.465	-426.761701[3]	-253.482114	**-233.585699**	**-230.663986**	9.61	21.83
57D	C_s	229	0.028		-252.749395	-232.226794	-229.557450	21.83	
58A	C_s	267		**-449.432282**	-253.758845[1]				4.05
58B	C_{3v}	246	10.585	-442.501104[1]	**-263.410755**	-237.898423	-225.469489	4.05	9.53
58C	D_{3h}	237	1.467		-260.086805	**-238.658866**	**-234.809078**	9.53	14.63
58D	C_1	235	0.465		-257.876211	-237.631296	-234.671473	14.63	14.94
58E	C_{3v}	234	0.027		-258.241372	-237.298283	-234.569986	14.94	
59A	C_{3v}	267		**-459.509280**	-260.795085[1]				3.77
59B	C_{2v}	272		-459.250400	-261.475383[2]			3.77	4.26
59C	C_1	250	10.832		-267.857802	-241.705877	-229.053528	4.26	4.86
								7.93	9.09
59D	C_{2v}	250	10.939	-453.109891[2]	**-267.945226**	-241.627254	-228.849111	4.86	7.93
59E	T_d	240	0.027		-264.710286	**-243.330508**	**-240.572493**	9.09	
60A	C_s	278		**-470.448485**					4.51
60B	C_s	255	11.042		**-273.341243**	-246.579281	-233.702420	4.51	9.29
60C	C_{2v}	246	1.470		-269.958055	-247.763712	-243.823553	9.29	9.85
60D	C_s	245	0.540		-269.408035	**-247.785988**	-244.566234	9.85	11.00
60E	C_{2v}	245	0.536		-269.292014	-247.781611	-244.572017	11.00	13.95
60F	C_s	244	0.027		-269.050233	-247.370671	**-244.579066**	13.95	
61A	T_d	284		**-482.025765**	-271.692826				4.65
61B	C_{2v}	260	11.174		**-278.726626**	-251.502374	-238.498558	4.65	9.54
61C	C_{3v}	249	0.027		-274.114496	**-252.402685**	**-249.587740**	9.54	
62A	C_s	293		**-491.052378**	-272.267523				4.00
62B	C_s	264	11.707	-485.425587[3]	**-283.183002**	-255.038209	-241.549494	4.00	6.33
62C	C_{2v}	264	11.174		-283.102592	-255.558891	-242.509563	6.33	9.22
62D	C_{2v}	255	1.473		-279.826688	-256.868159	-252.837765	9.22	9.64
62E	C_1	254	0.623		-279.851878	-256.899841	-253.442114	9.64	9.78
62F	C_s	254	0.560		-279.460422	**-256.908198**	-253.554702	9.78	10.47
62G	C_1	254	0.526		-279.357773	-256.897318	**-253.612942**	10.47	14.14
62H	C_1	253	0.027		-278.499195	-256.445284	-253.594448	14.14	
63A	C_s	301		**-501.731893**					3.83
63B	C_1	269	11.880	-497.181562	**-288.560948**	-259.921304	-246.279386	3.83	8.87
63C	C_s	259	0.533	495.356854[1]	-285.141958	**-262.030007**	**-258.620607**	8.87	14.14
63D	C_s	258	0.027		-283.876854	-261.487847	-258.601156	14.14	
64A	D_{3d}	307		**-512.831683**					3.85
64B	C_s	274	12.066	-503.234962	**-293.931716**	-264.790492	-250.989419	3.85	8.22
64C	C_{2v}	265	0.552	-501.818445[4]	-291.412250	**-268.023828**	**-264.587042**	8.22	24.31
64D	C_s	262	0.031		-289.333587	-265.722635	-262.644509	24.31	

TABLE I. continued

	PG	n_{nn}	E_{strain}	$\rho_0 = 3$	$\rho_0 = 6$	$\rho_0 = 10$	$\rho_0 = 14$	ρ_{min}	ρ_{max}
65A	C_s	310		**-523.446427**					3.86
65B	C_1	278	12.494		-298.321863	-268.406866	-254.407364	3.86	4.74
65C	C_2	278	12.574	-515.414573	**-298.392345**	-268.351634	-254.301092	4.74	6.32
65D	C_1	278	12.081		-298.317501	-268.836726	-254.984242	6.32	8.12
65E	C_{2v}	269	0.603		-296.317862	**-272.098786**	-268.513581	8.12	10.53
65F	C_1	269	0.565		-296.027614	-272.083782	-268.578320	10.53	11.30
65G	C_1	269	0.552		-295.806729	-272.069820	**-268.594702**	11.30	19.71
65H	C_s	267	0.027		-293.637761	-270.572952	-267.614569	19.71	
66A	C_s	314		**-534.464040**					3.82
66B	C_1	284	15.128	-530.516639	-303.512725	-271.712472	-256.391481	3.82	4.83
66C	C_1	283	12.758	-528.936842	**-303.763297**	-273.223079	-259.078765	4.83	7.83
66D	C_s	274	0.640		-301.866029	-277.134660	-273.454381	7.83	9.74
66E	C_s	274	0.573		-301.464889	**-277.145223**	-273.573502	9.74	11.50
66F	C_s	274	0.552		-301.193166	-277.115736	**-273.602343**	11.50	24.31
66G	C_s	271	0.033		-299.437330	-274.866840	-271.669464	24.31	
67A	C_s	318		**-544.754257**	-297.547886				3.80
67B	C_s	289	15.345	-539.666842[2]	-308.979846	-276.564507		3.80	5.46
67C	C_2	288	12.945	-538.179357[1]	**-309.130322**	-278.090470	-263.853175	5.46	7.72
67D	C_{2v}	279	0.677		-307.349356	**-282.171568**	-278.396059	7.72	11.36
67E	C_{2v}	279	0.674		-307.234099	-282.166219	**-278.400953**	11.36	21.85
67F	C_{3v}	276	0.033		-304.922619	-279.938518	-276.682086	21.85	
68A	C_s	324		**-555.582496**					3.68
68B	C_1	294	15.980	-551.451174	**-314.374880**	-281.011142	-265.753769	3.68	7.29
68C	C_s	293	12.938	-549.985909[1]	-314.146641	-281.905282	-267.100885	7.29	7.78
68D	C_1	283	0.666		-311.913082	-286.249826	-282.429781	7.78	9.67
68E	C_{2v}	283	0.597		-311.515987	**-286.263045**	-282.554370	9.67	11.24
68F	C_s	283	0.573		-311.246697	-286.237292	-282.588836	11.24	11.51
68G	C_{2v}	283	0.552		-310.973538	-286.207609	-282.617642	11.51	13.46
68H	C_{3v}	282	0.032		-311.238864	-285.954388	**-282.683003**	13.46	
69A	C_1	329		**-566.364140**	-307.245602				3.65
69B	C_1	308		-560.639499	-318.205833			3.65	4.22
69C	C_{5v}	298	14.909	-559.783221[1]	-319.687802	-286.265131		4.22	5.22
69D	C_s	299	16.223		**-319.819905**	-285.836885[1]		5.22	7.64
69E	C_s	288	0.705		-317.396150	-291.284253	-287.366805	7.64	9.66
69F	C_1	288	0.653		-317.293147	**-291.294050**	**-287.462110**	9.66	18.06
69G	C_1	286	0.034		-315.861945	-290.031196	-286.695880	18.06	
70A	C_{2v}	335		**-577.739782**					3.22
70B	C_1	332		-577.286914	-313.362561			3.22	3.67
70C	C_5	314		-571.815209	-324.211871			3.67	4.16
70D	C_{5v}	304	15.324	-570.747100	**-325.887749**	-291.872039		4.16	7.89
70E	C_s	293	0.676		-323.082118	**-296.412149**	-292.439398	7.89	12.18
70F	C_1	293	0.659		-322.802226	-296.365659	**-292.462856**	12.18	17.96
70G	C_s	291	0.035		-321.499078	-295.108247	-291.708765	17.96	
71A	C_1	330		**-588.396687**	-316.491227				3.42
71B	C_5	320		-583.202864	-330.363241			3.42	4.28
71C	C_{5v}	310	17.608	-581.944905[1]	**-331.588748**	-295.611936[2]		4.28	7.29
71D	C_{2v}	299	0.695		-329.356130	**-302.405357**	**-298.405353**	7.29	21.50
71E	C_s	296	0.034		-326.944961	-300.178953	-296.721356	21.50	
72A	C_1	335		**-599.690310**	-320.666142				3.40
72B	C_1	314	17.960	-595.064909	-335.877119	-299.300783	-283.195227	3.40	4.77
72C	C_s	313	16.818	-592.641021	**-336.121753**	-299.750026	-283.664026	4.77	7.29
72D	C_1	303	0.713		-333.967611	**-306.460206**	-302.387256	7.29	10.53
72E	C_1	303	0.695		-333.804475	-306.453999	**-302.413229**	10.53	21.49
72F	C_s	300	0.038		-331.710111	-304.261423	-300.734505	21.49	

TABLE I. continued.

	PG	n_{nn}	E_{strain}	$\rho_0 = 3$	$\rho_0 = 6$	$\rho_0 = 10$	$\rho_0 = 14$	ρ_{min}	ρ_{max}
73A	C_3	339		**-610.936684**	-324.743483				3.50
73B	C_s	319	18.316	-603.873759[2]	**-341.266253**	-304.026668	-287.806170	3.50	6.97
73C	C_s	318	16.192	-602.726569[2]	-340.979140	-305.189678	-289.451450	6.97	7.03
73D	C_s	308	0.725		-339.404682	**-311.517522**	-307.374386	7.03	10.72
73E	C_s	308	0.695		-339.241592	-311.502535	**-307.421094**	10.72	21.49
73F	C_1	305	0.037		-337.195061	-309.332640	-305.747113	21.49	
74A	C_{3v}	357		**-622.679870**					3.92
74B	C_s	324	18.513	-614.020203[2]	**-346.610834**	-308.886442		3.92	6.83
74C	C_{5v}	313	0.699	-610.492247[3]	-345.199617	**-316.650760**	**-312.441302**	6.83	21.38
74D	C_s	310	0.036		-342.649207	-314.403461	-310.759707	21.38	
75A	C_s	364		**-633.513370**					3.70
75B	C_1	328	18.559	-630.521082	-351.177041	-312.987148	-296.598914	3.70	5.81
75C	D_{5h}	319	0.718		**-351.472365**	**-322.643558**	**-318.407330**	5.81	21.14
75D	C_s	316	0.035		-348.965031	-320.414355	-316.759660	21.14	
76A	C_s	370		**-644.951602**					3.56
76B	C_1	334	21.847	-642.129130	-355.970657	-315.525026	-298.048750	3.56	4.16
76C	C_1	333	19.297	-641.559041	-356.249587	-317.224994	-300.488549	4.16	4.40
76D	C_1	333	19.272	-639.714777	**-356.372708**	-317.247110	-300.338642	4.40	6.17
76E	C_s	323	0.737		-356.085310	**-326.697484**	-322.386901	6.17	10.93
76F	C_{2v}	323	0.718		-355.771608	-326.682964	**-322.414257**	10.93	21.14
76G	C_1	320	0.035		-353.408271	-324.459592	-320.766507	21.14	
77A	C_1	368		**-656.079789**	-349.695795				3.68
77B	C_s	339	22.562	-650.115580[2]	-361.292679	-319.897701[2]		3.68	4.97
77C	C_1	338	19.477		**-361.727086**	-322.095213	-305.018458	4.97	6.12
77D	C_{2v}	328	0.749		-361.520971	**-331.753953**	**-327.371999**	6.12	20.66
77E	C_s	325	0.035		-358.839797	-329.504700	-325.773351	20.66	
78A	C_3	384		**-667.576295**					3.54
78B	C_1	344	22.724	-664.005603	-366.727436	-324.814567	-307.287362	3.54	5.18
78C	C_1	344	22.651		**-366.761455**	-324.883480	-307.076218	5.18	6.04
78D	C_s	338	11.849		-366.722670	-330.163464	-315.401197	6.04	6.53
78E	C_1	332	0.769		-366.132260	**-335.806666**	-331.349274	6.53	10.71
78F	C_s	332	0.749	-650.435529[3]	-365.871754	-335.796094	**-331.379143**	10.71	16.79
78G	C_1	330	0.037		-364.447522	-334.579848	-330.786061	16.79	
79A	C_1	385		**-678.940231**	-358.579695				3.59
79B	C_{2v}	348	19.381	-673.564685	**-372.832290**	-332.365043		3.59	6.53
79C	C_{2v}	343	11.973		-372.465769	-335.139012	-320.222688	6.53	6.67
79D	C_{2v}	337	0.783	-663.444178	-371.568226	**-340.862137**	-336.332369	6.67	11.06
79E	C_s	337	0.752	-659.185953[3]	-371.199420	-340.834084	-336.380124	11.06	11.48
79F	D_{3h}	336	0.036	-661.623659[2]	-370.982315	-340.653542	**-336.798725**	11.48	
80A	C_3	387		**-690.577890**					3.53
80B	C_s	354	21.858	-683.220844[2]	**-378.333471**	-335.897891[1]		3.53	6.36
80C	C_1	348	12.120		-377.972497	-340.072278	-324.944256	6.36	7.34
80D	C_1	341	0.806	-674.292236	-376.175628	**-344.911381**	-340.304108	7.34	10.44
80E	C_s	341	0.783		-375.919374	-344.904384	-340.339544	10.44	11.02
80F	C_s	341	0.752	-668.581802[4]	-375.572469	-344.877983	-340.387336	11.02	11.36
80G	C_s	340	0.040		-375.635945	-344.728294	**-340.811371**	11.36	

[1] J. Farges, M. F. de Feraudy, B. Raoult, and G. Torchet, Adv. Chem. Phys. **70**, 45 (1988).

[2] T. P. Martin, Phys. Rep. **273**, 199 (1996).

[3] S. J. Riley, in *Clusters of atoms and molecules II*, edited by H. Haberland (Springer-Verlag, Berlin, 1994), p. 221.

[4] S. E. Apsel, J. W. Emmert, J. Deng, and L. A. Bloomfield, Phys. Rev. Lett. **76**, 1441 (1996).

[5] S. Kakar *et al.*, Phys. Rev. Lett. **78**, 1675 (1997).

[6] J. A. Northby, J. Chem. Phys. **87**, 6166 (1987).

[7] J. P. K. Doye and D. J. Wales, Chem. Phys. Lett. **247**, 339 (1995).

[8] E. K. Parks, L. Zhu, J. Ho, and S. J. Riley, J. Chem. Phys. **100**, 7206 (1994).
[9] E. K. Parks and S. J. Riley, Z. Phys. D **33**, 59 (1995).
[10] E. K. Parks, L. Zhu, J. Ho, and S. J. Riley, J. Chem. Phys. **102**, 7377 (1995).
[11] E. K. Parks, G. C. Niemann, K. P. Kerns, and S. J. Riley, J. Chem. Phys. **107**, 1861 (1997).
[12] T. D. Klots, B. J. Winter, E. K. Parks, and S. J. Riley, J. Chem. Phys. **95**, 8919 (1991).
[13] M. Pellarin *et al.*, Chem. Phys. Lett. **217**, 349 (1994).
[14] M. S. Stave and A. E. DePristo, J. Chem. Phys. **97**, 3386 (1992).
[15] T. L. Wetzel and A. E. DePristo, J. Chem. Phys. **105**, 573 (1996).
[16] N. N. Lathiotakis, A. N. Andriotis, M. Menon, and J. Connolly, J. Chem. Phys. **104**, 992 (1996).
[17] J. M. Montejano-Carrizales, M. P. I. niguez, J. A. Alonso, and M. J. Lopez, Phys. Rev. B **54**, 5961 (1996).
[18] W. Hu, L. Mei, and H. Li, Solid State Commun. **100**, 129 (1996).
[19] S. K. Nayak, S. N. Khanna, B. K. Rao, and P. Jena, J. Phys. Chem. **101**, 1072 (1997).
[20] D. J. Wales and J. P. K. Doye, in preparation (1997).
[21] A. L. Mackay, Acta Cryst. **15**, 916 (1962).
[22] O. Echt, K. Sattler, and E. Recknagel, Phys. Rev. Lett. **47**, 1121 (1981).
[23] I. A. Harris, R. S. Kidwell, and J. A. Northby, Phys. Rev. Lett. **53**, 2390 (1984).
[24] I. A. Harris, K. A. Norman, R. V. Mulkern, and J. A. Northby, Chem. Phys. Lett. **130**, 316 (1986).
[25] T. P. Martin, T. Bergmann, H. Göhlich, and T. Lange, Chem. Phys. Lett. **172**, 209 (1990).
[26] T. P. Martin, T. Bergmann, H. Göhlich, and T. Lange, Chem. Phys. Lett. **176**, 343 (1991).
[27] T. P. Martin *et al.*, Chem. Phys. Lett. **183**, 119 (1991).
[28] O. Echt *et al.*, J. Chem. Soc., Faraday Trans. **86**, 2411 (1990).
[29] T. P. Martin, U. Näher, H. Schaber, and U. Zimmermann, Phys. Rev. Lett. **70**, 3079 (1993).
[30] L. D. Marks, Rep. Prog. Phys. **57**, 603 (1994).
[31] R. L. Whetten *et al.*, Adv. Mater. **8**, 428 (1996).
[32] R. P. Andres *et al.*, Science **273**, 1690 (1996).
[33] M. M. Alvarez *et al.*, Chem. Phys. Lett. **266**, 91 (1997).
[34] C. L. Cleveland *et al.*, Z. Phys. D **40**, 503 (1997).
[35] C. L. Cleveland *et al.*, Phys. Rev. Lett. **79**, 1873 (1997).
[36] B. Raoult, J. Farges, M. F. de Feraudy, and G. Torchet, Phil. Mag. B **60**, 881 (1989).
[37] J. Pillardy and L. Piela, J. Phys. Chem. **99**, 11805 (1995).
[38] J. P. K. Doye, D. J. Wales, and R. S. Berry, J. Chem. Phys. **103**, 4234 (1995).
[39] P. A. Braier, R. S. Berry, and D. J. Wales, J. Chem. Phys. **93**, 8745 (1990).
[40] I. Bytheway and D. L. Kepert, J. Math. Chem. **9**, 161 (1992).
[41] J. P. K. Doye and D. J. Wales, Science **271**, 484 (1996).
[42] J. P. K. Doye and D. J. Wales, J. Phys. B **29**, 4859 (1996).
[43] D. J. Wales and J. P. K. Doye, in *Large Clusters of Atoms and Molecules*, Vol. E 313 of *NATO ASI*, edited by T. P. Martin (Kluwer Academic, Dordrecht, 1996), pp. 241–279.
[44] C. Rey and L. J. Gallego, Phys. Rev. E **53**, 2480 (1996).
[45] D. T. Mainz and R. S. Berry, Mol. Phys. **88**, 709 (1996).
[46] M. R. Hoare and J. McInnes, J. Chem. Soc., Faraday Discuss. **61**, 12 (1976).
[47] M. R. Hoare and J. McInnes, Adv. Phys. **32**, 791 (1983).
[48] M. H. J. Hagen and D. Frenkel, J. Chem. Phys. **101**, 4093 (1994).
[49] P. M. Morse, Phys. Rev. **34**, 57 (1929).
[50] D. J. Wales, L. J. Munro, and J. P. K. Doye, J. Chem. Soc., Dalton Trans. 611 (1996).
[51] L. A. Girifalco, J. Phys. Chem. **96**, 858 (1992).
[52] D. J. Wales and J. Uppenbrink, Phys. Rev. B **50**, 12342 (1994).
[53] L. A. Girifalco and V. G. Weizer, Phys. Rev. **114**, 687 (1959).
[54] J. E. Jones and A. E. Ingham, Proc. R. Soc. A **107**, 636 (1925).
[55] T. Kihara and S. Koba, J. Phys. Soc. Jpn. **7**, 348 (1952).
[56] L. D. Marks, Phil. Mag. A **49**, 81 (1984).
[57] C. L. Cleveland and U. Landman, J. Chem. Phys. **94**, 7376 (1991).
[58] W. H. Press *et al.*, *Numerical Recipes* (Cambridge University Press, Cambridge, 1986).
[59] C. J. Cerjan and W. H. Miller, J. Chem. Phys. **75**, 2800 (1981).
[60] T. Coleman and D. Shalloway, J. Global Optimization **4**, 171 (1994).
[61] G. L. Xue, J.Global Optimization **4**, 425 (1994).
[62] D. M. Deaven, N. Tit, J. R. Morris, and K. M. Ho, Chem. Phys. Lett. **256**, 195 (1996).
[63] D. J. Wales and J. P. K. Doye, J. Phys. Chem. A **101**, 5111 (1997).
[64] J. P. K. Doye and D. J. Wales, Z. Phys. D **40**, 194 (1997).
[65] G. T. Barkema and N. Mousseau, Phys. Rev. Lett. **77**, 4358 (1996).
[66] J. P. K. Doye and D. J. Wales, Phys. Rev. Lett. submitted (1997).
[67] F. H. Stillinger and D. K. Stillinger, J. Chem. Phys. **93**, 6106 (1990).
[68] D. J. Wales, J. Chem. Phys. **101**, 3750 (1994).
[69] J. Rose and R. S. Berry, J. Chem. Phys. **98**, 3262 (1993).
[70] J. P. K. Doye and D. J. Wales, J. Chem. Phys. **105**, 8428 (1996).
[71] K. Clemenger, Phys. Rev. B **32**, 1359 (1985).
[72] J. P. K. Doye and D. J. Wales, Chem. Phys. Lett. **262**, 167 (1996).
[73] U. Zimmermann *et al.*, Phys. Rev. Lett. **72**, 3542 (1994).
[74] M. Sung, R. Kawai, and J. H. Weare, Phys. Rev. Lett. **73**, 3552 (1994).
[75] R. Poteau and F. Spiegelmann, J. Chem. Phys. **98**, 6540 (1993).
[76] D. Rayane *et al.*, Phys. Rev. A **39**, 6056 (1989).
[77] W. N. Lipscomb, Science **153**, 373 (1966).
[78] A. Pinto *et al.*, Phys. Rev. B **51**, 5315 (1995).
[79] G. Schmid, Chem. Rev. **92**, 1709 (1992).
[80] J. Xie, J. A. Northby, D. L. Freeman, and J. D. Doll, J. Chem. Phys. **91**, 612 (1989).
[81] J. Uppenbrink and D. J. Wales, J. Chem. Phys. **96**, 8520 (1992).
[82] Q. Wang, M. D. Glossman, M. P. Iniguez, and J. A. Alonso, Phil. Mag. B **69**, 1045 (1994).

[83] H. S. Lim, C. K. Ong, and F. Ercolessi, Surf. Sci. **269/270**, 1109 (1992).
[84] G. Schmid *et al.*, Chem. Ber. **114**, 3634 (1981).
[85] L. R. Wallenberg, J. O. Bovin, and G. Schmid, Surf. Sci. **156**, 256 (1985).
[86] H. C. D. H. Rapoport, W. Vogel and R. Schlögl, J. Phys. Chem. **101**, 4175 (1997).
[87] F. C. Frank and J. S. Kasper, Acta Cryst. **11**, 184 (1958).
[88] F. C. Frank and J. S. Kasper, Acta Cryst. **12**, 483 (1959).
[89] M. F. Ashby, F. Spaepen, and S. Williams, Acta Metall. **20**, 1647 (1978).
[90] C. L. Henley and V. Elser, Phil. Mag. B **53**, L59 (1986).
[91] V. A. Borodin and V. M. Manichev, Phys. Rev. B **54**, 15747 (1996).
[92] C. Lüder, D. Prekas, and M. Velegrakis, Laser Chem. **17**, 109 (1997).
[93] D. R. Nelson and F. Spaepen, Solid State Phys. **42**, 1 (1989).
[94] J. D. Bernal, Nature **185**, 68 (1960).
[95] J. D. Bernal, Proc. Royal Soc. A **280**, 299 (1964).
[96] G. S. Cargill, Solid State Phys. **30**, 227 (1975).
[97] H. Jonsson and H. C. Andersen, Phys. Rev. Lett. **60**, 2295 (1988).
[98] D. R. Nelson, Phys. Rev. Lett. **50**, 982 (1983).
[99] D. R. Nelson, Phys. Rev. B **28**, 5515 (1983).
[100] M. D. Glossman, J. A. Alonso, and M. P. Iñiguez, Phys. Rev. B **47**, 4747 (1993).
[101] W. D. Knight *et al.*, Phys. Rev. Lett. **52**, 2141 (1984).
[102] J. Pedersen *et al.*, Nature **353**, 733 (1991).
[103] N. Pavloff and S. C. Creagh, Phys. Rev. B **48**, 18164 (1993).
[104] J. P. K. Doye and D. J. Wales, J. Chem. Phys. **102**, 9659 (1995).
[105] In ref. 38, $\gamma(E')_s$ incorrectly appeared in the equation for $p_i(E)$, the probability that the cluster resides in region i of configuration space.
[106] J. P. K. Doye, A. Dullweber, and D. J. Wales, Chem. Phys. Lett. **269**, 408 (1997).
[107] D. J. Wales, J. Chem. Soc., Faraday Trans. **86**, 3505 (1990).
[108] J. P. K. Doye and D. J. Wales, J. Chem. Soc., Faraday Trans. **88**, 3295 (1992).
[109] D. J. Wales, J. P. K. Doye and A. Dullweber, The Cambridge Cluster Database, URL <http://brian.ch.cam.ac.uk/CCD.html>.